Building and Environment 184 (2020) 107180

Contents lists available at ScienceDirect

Building and Environment

journal homepage: http://www.elsevier.com/locate/buildenv

Integration of the WUDAPT, WRF, and ENVI-met models to simulate extreme daytime temperature mitigation strategies in San Jose, California

Ian McRae [a,*], Frank Freedman [b], Ana Rivera [c], Xinwei Li [d], Jingjing Dou [e], Isa Cruz [b], Chao Ren [d], Iryna Dronova [a,f], Harrison Fraker [g], Robert Bornstein [b]

[a] Department of Landscape Architecture and Environmental Planning, College of Environmental Design, UC Berkeley, USA
[b] Department of Meteorology and Climate Sciences, SJ State University, San Jose, USA
[c] Department of Geography and Global Studies, SJ State University, San Jose, USA
[d] Department of Architecture, The University of Hong Kong, Hong Kong, China
[e] Institute of Urban Meteorology, Chinese Meteorological Agency, Beijing, China
[f] Department of Environmental Science, Policy & Management, Rausser College of Natural Resources, UC Berkeley, USA
[g] Department of Architecture, College of Environmental Design, UC Berkeley, USA

ARTICLE INFO

Keywords:
WUDAPT
Urbanized WRF
ENVI-met
Urban heat islands
Urban planning
Thermal mitigation strategies

ABSTRACT

An obstacle to the modeling of strategies to mitigate extreme urban temperatures is frequently the lack of on-site meteorological data. The current study thus reports on a method that used the Weather Research and Forecasting (WRF) model to generate inputs for the ENVI-met model to produce building-scale canyon temperatures within a 300 m square near downtown San Jose. A land use distribution was generated for WRF by a WUDAPT classification, and the days of interest were then the hottest day in California history and a typical summer day. The source of meteorological data for ENVI-met, run with a 1.5 m cubic grid, was either an urbanized version of WRF; its default version; or observations at the closest NWS site. All WRF simulations were run on a 1 km grid, and output at its grid closest to the study area provided ENVI-met with lateral boundary conditions. The mitigation strategy was comprised of three parts, which either increased vegetation, rooftop albedo, or architectural shade elements. Results showed all strategies with only negligible impacts on ENVI-met nighttime 1 m level street canyon temperatures. Increased vegetation, however, was the most effective daytime strategy on both days, as it affected the largest area. The maximum vegetative cooling on the extreme and average days was −3.5 and −3.3 °C, respectively. While increased rooftop albedos produced near negligible impacts, increased architectural shading produced corresponding values of −1.6 and −1.7 °C, respectively.

1. Introduction

Over half the global population lives in cities susceptible to impacts from urban heat islands (UHIs), which may intensify due to greenhouse gas warming [61]. Alleviation of these effects by planning interventions is challenging due to the complexity of urban built features and due to their interactions with regional meteorological and climate change patterns. Although these phenomena have been studied extensively from the city-wide perspective by use of modeling and remote sensing techniques [65], specific contributions from local urban design to spatial patterns of extreme temperature are still poorly understood. An understanding of urban microclimates within changing regional climates requires consideration of the factors controlling both existing urban land cover patterns and the use of local design mechanisms.

Previous studies have primarily evaluated individual planning platforms [40], but few have investigated the downscaling of urban scale model outputs to neighborhood and building scale models [8,20]. Efforts are thus needed that first adopt an urban morphology extraction methodology, such as the World Urban Database and Access Portal Tools (WUDAPT) Level 0 method [10] to produce local climate zone (LCZ) distributions as inputs to an urban scale meteorological model, such as the Weather Research and Forecasting (WRF) model [55]. The procedure would then use WRF outputs as inputs to a micro-scale urban planning model, such as ENVI-met, to test impacts from various planning scenarios. Such studies would be useful to the professional planning fields (i.e., landscape and building architecture, as well as urban

* Corresponding author. Faculty of College of Environmental Design University of California, Berkeley 230 Wurster Hall #1800, Berkeley, CA, USA.
E-mail address: imcrae@berkeley.edu (I. McRae).

https://doi.org/10.1016/j.buildenv.2020.107180
Received 15 May 2020; Received in revised form 1 August 2020; Accepted 3 August 2020
Available online 16 August 2020

planning and design) as they become more reliant on computer models to guide decision making processes in their investigations of the 3-D interactions between built environments and their surroundings [64].

A diversity of software platforms exists to evaluate 3-D impacts on urban environmental factors that result from architectural and planning changes, e.g., impacts on human comfort and building energy consumption. Leading platforms include City Sim Pro, Rayman, Honeybee/Ladybug Plugins for Grasshopper, AutoDesk CFD, SOLWEIG, and ENVI-met. The most advanced of these models have a computational fluid dynamics (CFD) formulation, discussed below. These models have varying complexities and work on a range of scales (i.e., room to building to neighborhood). Their inputs generally include both meteorological parameters at a single site and 3-D urban morphological data, each with varying levels of detail.

Few applications have investigated meteorological linkages between the city wide meso-scale and the building microscale [6,25]. The Honeybee/Ladybug Plugin [44] generally is used to calculate indoor or outdoor thermal comfort. It accounts for shading, but does not consider vegetative evapotranspiration, longwave energy, or wind flow. While City Sim Pro [44] does simulate evapotranspiration processes, it does not include wind flow. It has been validated according to the Building Energy Simulation Test [32] and by EnergyPlus, a US Department of Energy model to simulate building energy usages [21].

Rayman [36] uses radiative fluxes and physiological indices to quantify outdoor human comfort, such as the Physiological Equivalent Temperature (PET) and Percent Mean Vote (PMV, [49]). While it accounts for longwave radiation exchanges, it does not consider wind flow. The Solar and Longwave Environmental Irradiance Geometry (SOLWEIG) model [39] simulates complex spatial radiation fluxes and shadow patterns but has only a limited ability to specify building materials properties. While it predicts human comfort, it does not consider air flow impacts [34].

The more advanced AutoDesk CFD model [2] calculates the temperatures of free-standing objects produced by convective flows, but it does not account for evapotranspiration [51]. Such models are comprised of 3-D prognostic equations for grid-point values of atmospheric: temperature (T, where all symbols are defined in the Appendix), wind speed (V) and direction (dd), specific humidity (q), and turbulent kinetic energy (TKE). While it has been used for indoor ventilation applications, it has not yet been validated for outdoor applications.

Most of the above limitations are overcome by the ENVI-met CFD model [13] that simulates at high spatial (0.5–10 m grids) and temporal (10 s) resolutions [43]. In additional to atmospheric variables, it also simulates leaf T, as well as vegetative energy and water vapor exchanges [54]. It has been used for studies of air quality [62] and pedestrian thermal comfort [4]. It has also been used to investigate UHIs. [24,45]. UHI mitigation strategies have also been studied, including park induced cool islands [18,37]; passive cooling systems [52,53]; urban canyon orientation and aspect ratio [33]; and material properties [63]. It has been validated against field measurements [59], showing that it can reasonably simulate air T, as well as building surface radiative T and energy balance components [68]. The model has thus been used in real urban planning applications [16]. It has had problems, however, with input wind speeds >2 m s^{-1} [20,56], and it also overestimates TKE production around physical objects [29]. The version used by allowed for only constant input values for all meteorological variables.

The required meteorological inputs for the ENVI-met initial (IC) and boundary (BC) conditions can come from the observations at a nearby site or from a mesoscale meteorological model (MMM), such as WRF. Observations can be from the closest official National Weather Service (NWS) site or a nearby local site [19]. WRF outputs for ENVI-met can either be from a simple urbanization parameterization, e.g., the Noah land use model [23]; or from one with a more complex formulation, e.g., its Single-Layer Urban Canopy Model (SLUCM) [35]. Its most realistic scheme is the multilevel Building Environment Parameterization (BEP) [42], coupled with its Building Energy Model (BEM) [50].

[38] used SLUCM + ENVI-met to study urban park impacts on UHI magnitude. Results showed that larger WRF domains produced more accurate microclimate projections, because impacts from surrounding terrain were incorporated. [20] used WRF + BEP + BEM with ENVI-met to investigate UHIs in Chicago in a changing climate. Their ENVI-met V3.1 could only be run in a steady state mode [41] and was run with an 1 h spin up. The WRF horizontal grid resolution was 0.33 km, while ENVI-met used a uniform 3-D 2-m grid spacing.

The required unprocessed land-use/land-cover (LU/LC) data for both the urban and rural sites in ENVI-met can be obtained either from local field observations, existing spatial products such as a National Land Cover Map, aerial photos, airborne lidar, satellite images, or detailed building records. Such building data are then processed by ArcGIS software to generate geo-referenced shape files or by manual analyses of building morphology via ENVI-met tools. [57] standardized the LCZ framework to classify a city and its surrounding areas into 17 LU/LC classes, based on four aspects of the urban buildings and trees: roughness, packing (i.e., density), ground cover (i.e., pervious vs. impervious), and thermal emittance. The WUDAPT Level 0 methodology produces an LCZ classification map for a city from satellite data and free software from [9]. Use of LCZ data in urbanized-WRF (herein uWRF) improves its accuracy [12,17].

The current study focuses on quantification of daytime urban temperature impacts from the application of a variety of thermal mitigation strategies. Whereas most previous such studies have primarily focused on the use of an individual research platform, few have investigated interactions over the range of urban scales from the downscaling of MMM outputs to a microscale CFD model. The current study thus first uses a WUDAPT Level 0 derived LCZ classification as input to uWRF, and then uses its time-varying meteorological output to drive the ENVI-met V4.3.0 CFD planning model in a series of 1 m level urban street canyon temperature mitigation scenarios. The aim of the study is thus to use the WUDAPT, uWRF, and ENVI-met models to answer the following research question: can meso-scale meteorological models be used in lieu of on-site observations to drive models for the evaluation of street canyon heat mitigation strategies for the reduction of summer daytime temperatures in an existing urban neighborhood?

2. Methodology

An overview of the current methodology (Fig. 1) shows the three possible sources of meteorological data used in any ENVI-met simulation: NWS observations, WRF, or uWRF. The Landsat LU/LC data are either fed directly into WRF or first processed by WUDAPT before ingestion by uWRF, while no such data are required for an NWS application. The ENVI-met simulations each utilize user generated LU/LC data, regardless of that used in the previous meteorological data step. Details are provided below.

2.1. Study site

The study focuses on a portion of San Jose, located on the Central Coast Region in the Santa Clara Valley (SCV, where all acronyms are defined in the Appendix), now the Silicon Valley (Fig. 2b). The Valley provides the main sea level entry for cool marine air into SJ (Fig. 2a). The SJ 2-m T-values are projected to increase by 2–3.5 °C by the end of the century, increasing its maximum annual heat wave frequency to 10 events [15]. Its bayside communities will see the greatest increase in regional mortality [14]. During a record breaking 10-day heat wave in July 2006, the Central Coast Region contributed 28% of all statewide excess emergency room visits and 47% of all excess hospitalizations, even with only 18% of the state population.

The ENVI-met study area is a 300 m square centered on the intersection of two major commercial boulevards, with a few surrounding residences (Fig. 2c). The site is a crowded shopping area and a gathering spot for local communities. Its off-core urban typology is common to

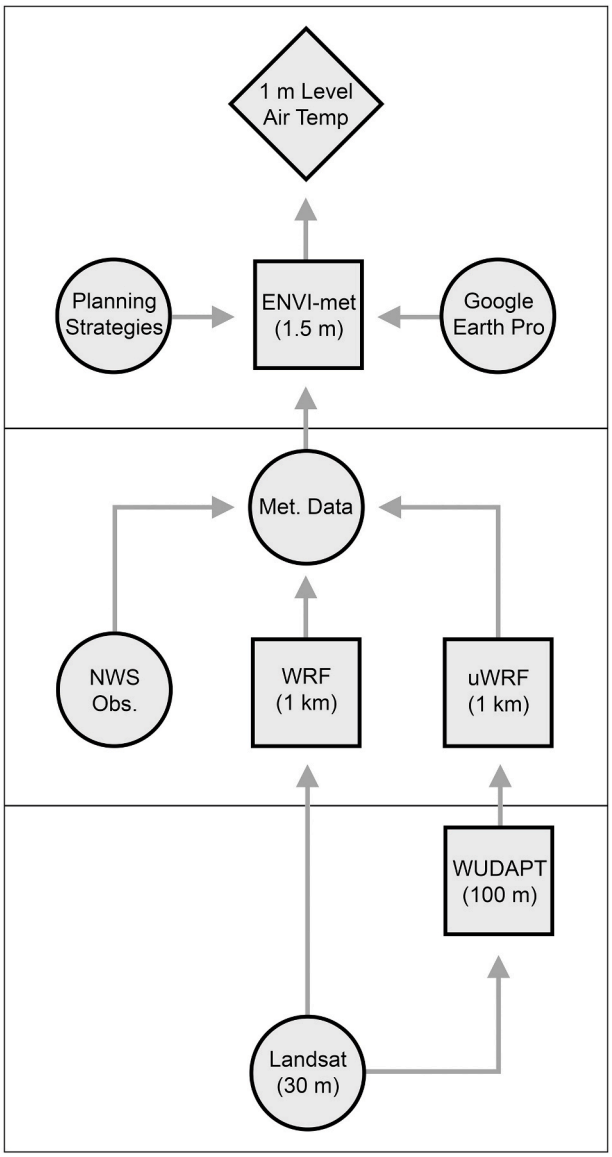

Fig. 1. Methodological overview, where squares represent models, circles are data sets, and the diamond is the final temperature (T) values. The lower box shows the LU/LC data used in the WRF models, the middle are the three possible meteorological data sets for an individual ENVI-met simulation, and the upper are the additional data sets ingested into ENVI-met to generate 1 m level temperatures (T). Numbers in parentheses give the spatial resolution in meters (m) of the output data.

many US and global cities: a mix of commercial and residential structures with sparse vegetative coverage. The day of interest is 1 September 2017, the hottest day in California history at that time, with a high T of 42°C (108°F) in SJ. The study thus evaluates ENVI-met performance under a variety of 1 m level urban canyon T-mitigation strategies for this cloudless "extreme" day and for 9 July 2017, a more "typical" cloudless summer day.

2.2. WUDAPT level 0 method

Various approaches exist to develop LCZ maps [3,27]. The current study uses the LCZ scheme of [58],which requires detailed urban morphological data. Such data can be hard to acquire, but the WUDAPT Level 0 methodology [9,10] creates an LCZ map using open satellite data and free software. The method has three steps: (i) data preprocessing, (ii) digitization and evaluation of sample training areas using Google Earth, and (iii) LCZ classification with SAGA GIS.

Landsat-8 Level-1 Terrain Corrected (LT1) data were acquired from the US Geological Service (USGS) for 30 August 2016 via the Earth Explorer portal. Landsat-8 has a spatial resolution of 30 m in both the visible Near Infrared (NIR) and Shortwave Infrared (SWIR) Bands, and a resolution of 100 m in the Thermal Band (TIR). All data were imported into SAGA GIS to be projected and clipped to the region of interest (ROI). At least 20 homogeneous training sample areas for each of the 17 built area LCZ classes within the ROI were identified and manually digitized via Google Earth. The unique spectral signals of each LCZ training class were identified and then used to classify a second group of known LCZ sites. Classification accuracy for the second group was evaluated via the SAGA Accuracy Matrix Polygon to Grid tool, which compares predicted LCZ class of each member of the second group against its training class. After several iterations, the final training class results were imported into the SAGA classification algorithm to classify the entire ROI.

These results were then resampled to produce a 100 m resolution LCZ map for the entire WRF domain. To create the required WRF input, the LCZ 100-m fields were aggregated to its 1 km grid, maintaining the 17-Category classifications. The class of each 1 km grid was assigned based on the most common LCZ class within that grid. Once aggregated, LCZ 3 areas (defined in Table 3) were assigned to the WRF-SLUCM Category 31 (defined in Table 2a); LCZ 6 areas were assigned to Category 32; and LCZs 4, 5, 7, 8, and 10 areas all went into Category 33.

2.3. WRF model

ENVI-met simulations for the extreme day evaluated three sources (top rows of Table 1) of input background meteorological data, ranked according to decreasing complexity: (i) *"Urban-WRF"* with its SLUCM urbanization parameterization and WUDAPT LU/LC data; (ii) *"Default-Urban"* with the default WRF urban configuration, i.e., a simple urban roughness length (z_0) parameterization, and only look-up table urban LU/LC information; and (iii) *"San Jose Mineta Airport"* (SJA, Fig. 2b) with only NWS surface observations, the most common ENVI-met input source type, and with upper level data from a Oakland International Airport (OIA, Fig. 2a) NWS radiosonde. Typical day simulations used only urban WRF outputs.

All WRF simulations used model Version 3.9 on a 1 km horizontal grid in the domain of Fig. 2b. All were forced at their lateral boundaries by 12-km analysis fields from the 2018 North American Mesoscale Forecast System Model (NAM), configured with 51 vertical levels, with the lowest at 30 m and with 14 below 2500 m. The Mellor-Yamada-Janjic PBL scheme was selected [31]. Initial soil moisture values for all land areas were lowered to 75% of the NAM monthly climatological values to optimize agreement between the 2-m WRF T-values and observations from the SJA and San Jose State University (SJSU) meteorological stations. The latter site is atop its Duncan Hall Science building, at 41 m (all heights herein are AGL). Such adjustments are commonly made for soil moisture, as local values are generally not well reproduced in WRF [20].

The *Default-Urban* simulation used the USGS 24-category LU/LC classification in WRF, with its only one urban class. These categories were compiled from 1993 Landsat data at a resolution of 30 m [11], and thus do not account for the newer built-up portions of SJ. Default (constant) WRF surface energy balance parameters for the one urban class include: z_0 of 0.5 m, heat capacity (C) of 10^6 J kg^{-1} K^{-1}, surface emissivity (ϵ) of 0.88, surface albedo (α) of 0.15, and soil thermal conductivity (k) of 3.24 W m^{-1} K^{-1}.

The SLUCM scheme used in the *Urban-WRF* simulations characterizes urban canopies via input building heights and widths; road widths; built fraction, among others. It distinguishes between the three urban land-use classes defined in Table 2a. Values for each urban canopy parameter are given in Table 2a as a function of land-use category. Their associated thermal and radiative parameters (independent of category) for the three built facets are given in Table 2b.

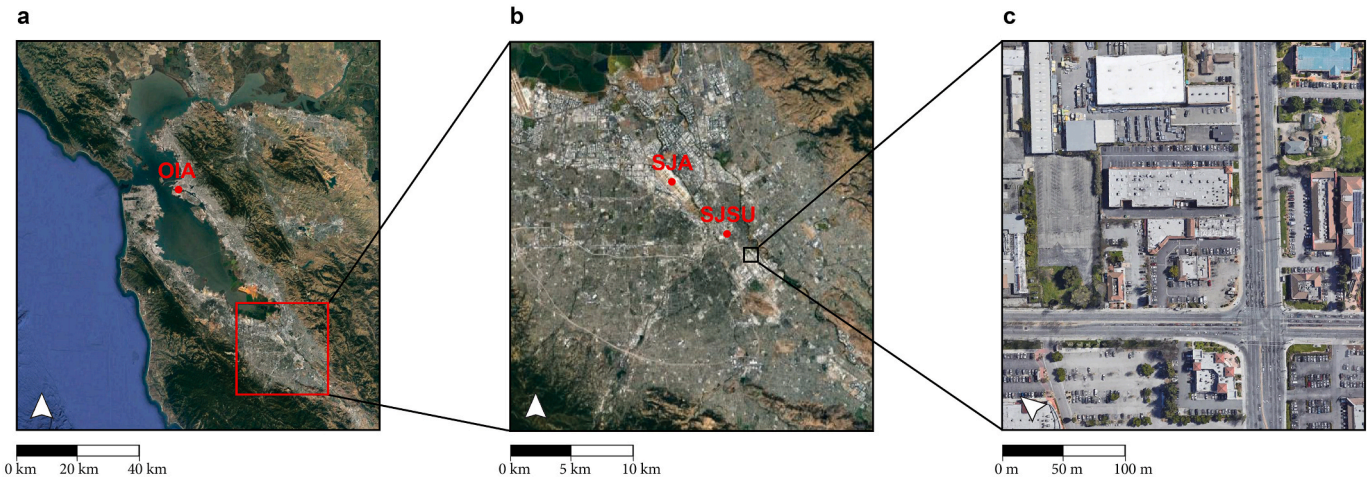

Fig. 2. Study area maps showing the: (a) San Francisco Bay Area, highlighting Oakland International Airport (OIA) and the city of San Jose (red box); (b) WRF domain, highlighting San Jose International Airport (SJA), San Jose State University (SJSU), and the ENVI-met study sub-area (red box); and (c) ENVI-met study-area, including the major intersection of McLaughlin Avenue and Story Road. (For interpretation of the references to color in this figure legend, the reader is referred to the Web version of this article.)

The single layer SLUCM, and not the multilayer BEP + BEM, urbanization scheme in WRF was used in the present study, as this exploratory study seeks to demonstrate the usefulness of the WUDAPT + WRF + ENVI-met model suite. While the BEP + BEM computational requirements far exceed those for SLUCM, the results (below) show that SLUCM can reasonably well reproduce key meteorological observations.

All extreme case WRF simulations for 1 September were run over a 96-h period from 0600 LST (= 1500 UTC) on 30 August to capture both the maximum T run-up and cool-down periods. The first 24-h were considered a spin-up period and were not considered. A similar approach was used for the typical day of 9 July.

2.4. ENVI-met model

Simulated air temperatures at the 1 m level from ENVI-met version 4.3.0 were analyzed in the current study, as it is the meteorological parameter most closely related to human heat stress [44]. It is also the one most accurately simulated by ENVI-met [30]. A grid spacing of 1.5 m used for each 3-D axis was a compromise between resolution and computation time [34]. The application used 20 vertical cells and 200 by 200 horizontal cells, with an additional five cell buffer zone at each lateral boundary, as recommended by [26]. The 3-D ENVI-met model top at 30 m is sufficient for this application, given the 14 m maximum building height in the computational domain and the recommended

Table 1
Meteorological (Met) model (WRF) or observational (Obs) input simulation-constants and hourly-variables ( )* for four groups of ENVI-met simulations, each for both daytime (1200–1500 LST) and nighttime (2000–2300 LST) hours on extreme and typical 2017 summer days. Values provide hourly lateral-boundary- and/or initial-conditions, and where LU/LC is Land-Use/Land-Cover, D is Day, N is Night, and PBL is planetary boundary layer. A description of each variable can be found in the text.

Inputs for ENVI-met simulations				
Simulation / Factor	San Jose Airport (Obs)	Default WRF	Urban WRF	Urban WRF
Temperature condition	Extreme	Extreme	Extreme	Typical
2017 date	1 Sept	1 Sept	1 Sept	9 July
Met model LC/LU data source	N/A	Default WRF	WUDAPT	WUDAPT
Solar transmissivity	1.00	0.89	0.89	0.92
PBL height (H, m)	Day 2500 Night 2500	Day 517 Night 32	Day 517 Night 32	Day 502 Night 31
Specific humidity at H (g kg^{-1})	Day 4.8 Night 4.8	Day 5.9 Night 6.9	Day 5.6 Night 7.3	Day 6.6 Night 7.6
10-m wind direction (deg)	Day 295 Night 180	Day 312 Night 232	Day 307 Night 202	Day 320 Night 299
2-m air temperature (°C)*	Min 31 Max 42	Min 30 Max 42	Min 29 Max 41	Min 20 Max 31
2-m relative humidity (%)*	Min 14 Max 31	Min 14 Max 26	Min 13 Max 30	Min 22 Max 54

Table 2a
Input parameters for *Urban-WRF* as a function of building class (i.e., 31, 32, and 33), where sensible and latent heats are both anthropogenic flux components and where σ is standard deviation.

Class / Factors	Newer Residential 31	Older Residential 32	Industrial/Commercial 33
Building height (h, m)	6.5	5.5	7.5
σ of h (m)	1	1	2
Roof width (m)	8.3	8.3	10.0
Sensible heat (W m^{-2})	20	20	90
Latent heat (W m^{-2})	20	20	40
Urban fraction	0.75	0.50	0.95

factor of two for this ratio.

The ENVI-met initialization begins with a single observed or WRF output value of 2-m level T and RH (which allow for computation of q), as well as 10 m level wind V and dd. The model then calculates a 1-D (vertical) solution to its prognostic equations to a PBL height of 2.5 km, but with dd held constant with height. These profiles then initialize the 3-D model, but with additional steps for wind velocity. The first step is without obstacles, while the second and final steps set built densities at 50 and 100% of their true values, respectively. Simple-forced lateral BCs were selected, so that at each time step (Δt) the current 1-D model solution T and q was applied to all inflow lateral boundaries.

Forcing (or nudging) increases model accuracy and thus ENVI-met results on all inflow boundaries at each Δt are nudged by either (interpolated from hourly input) observations or WRF output, dependent on the simulation. Nudged parameters included 2-m level T and RH, which allowed for computation of 2 m values of q. Although later model versions now support it, 10 m level V and dd values were not forced in the current study. Although observed 10-m V-values ranged from 0.9 to 4.5 m s^{-1}, a constant BC value of 1.5 m s^{-1} was used for all simulations at all heights, given the numerical problems previously reported with higher speeds. While this assumption overestimates maximum T values due to reduced ventilation, it likewise maximizes T-mitigation impacts. To create vertical profiles, T is assumed to decrease adiabatically (at 10 K km^{-1}), while q was assumed constant with height. Over the 30 m depth of the 3-D model, these assumptions should be reasonable. Further details on the entire BC process can be found in [29].

Satellite imagery within Google Earth Pro software produced building footprints and elevations, as well as vegetation types and distributions, within the model domain (Fig. 3). Users analyze images with AutoCAD to delineate existing and proposed LU/LC surface features, from which footprint surface areas are calculated. Results showed the study area with 26 buildings (Fig. 3a) ranging in height from 5 to 14 m, as well as with 217 trees ranging in height from 1 to 18 m. The figure (by % of area) shows the site characterized by a low building-density, many parking lots, and moderate vegetative (tree canopy and permeable surfaces) coverage. The remaining 22% is mostly roadways and sidewalks. Where trees overlapped buildings, the latter took precedence.

The temperature mitigation strategy was comprised of three sub-strategies that increased vegetation, rooftop albedo, or architectural shade elements. To achieve the 30% vegetation cover required to significantly reduce temperatures [46], current green coverages (Fig. 3a) were increased (Fig. 3b). This involved increasing street-tree number and density, greening building facades, and converting a vacant lot into a park. An increased ground surface α was not implemented, as that would increase pedestrian thermal loads. The roof top sub-strategy assumed that the current rooftop (terracotta tiles, asphalt shingles, and flat bitumen) α-value of 0.5 would be increased to 0.9 [60]. A value of 1.0 was not used to reflect weathering effects. All other rooftop physical and thermal properties were left at their default ENVI-met values.

The final sub-strategy was architectural shade structures, i.e., solar panels and one large light-weight polyvinyl chloride (PVC) shade cloth. Solar panel orientation followed the predominantly north-south or east-west orientation of the newly covered parking spaces. Panels were set 7 m high, were 6 m deep, had a width of 3 m per adjacent parking spots, and were composed of glass, silicon, and steel. Nearly every parking space in the site was shaded, amounting to 7% coverage. The PVC shade cloth was implemented over the intersection of Story Road and McLaughlin Avenue, the major intersection in Fig. 2c. The cloth amounted to 2% coverage, was a 38 m square, and was suspended at 10

Table 2b
Energy balance parameters for *Urban-WRF* as a function of built facets, independent of building class.

Parameter / Facet	Heat Capacity (10^6 J m^{-3} K^{-1})	Thermal Conductivity (J m^{-1} s^{-1} K^{-1})	Albedo (-)	Surface Emissivity (-)
Walls	1.75	1.50	0.05	0.98
Roofs	1.75	1.20	0.05	0.90
Ground	1.75	1.50	0.05	0.98

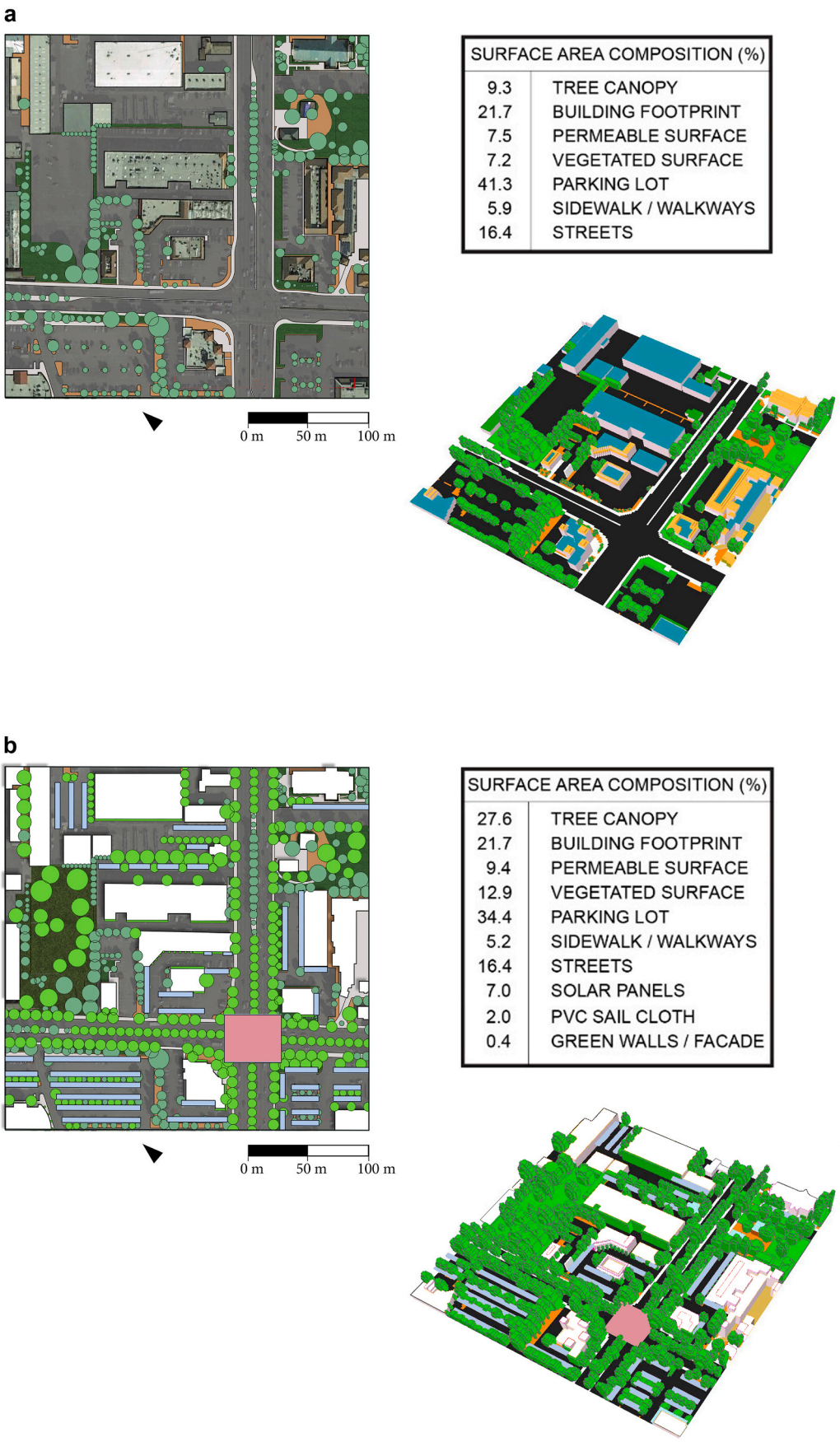

Fig. 3. ENVI-met study-site surface area LU/LC distributions in plan and 3-D perspectives: (a) for existing conditions and (b) after application of all three heat mitigation strategies discussed in the text.

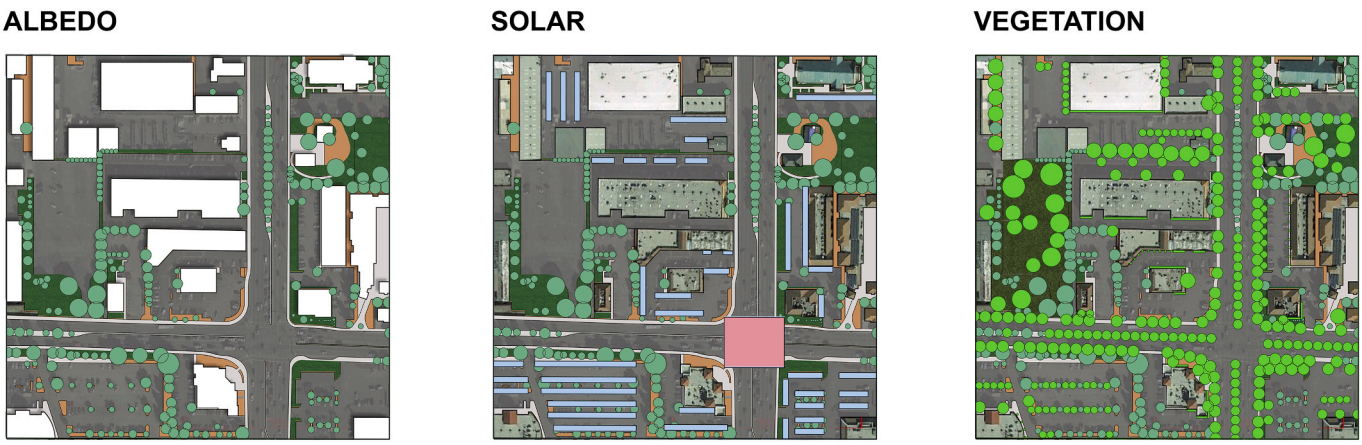

Fig. 4. Same plan view as in Fig. 3, but after application of each mitigation strategy that comprises the "combined" strategy in Fig. 3, including increased: rooftop albedos (left; white areas), solar panel and sail cloth shading (middle; grey and pink areas, respectively), and vegetative greening (right). See text for explanation of each strategy. (For interpretation of the references to color in this figure legend, the reader is referred to the Web version of this article.)

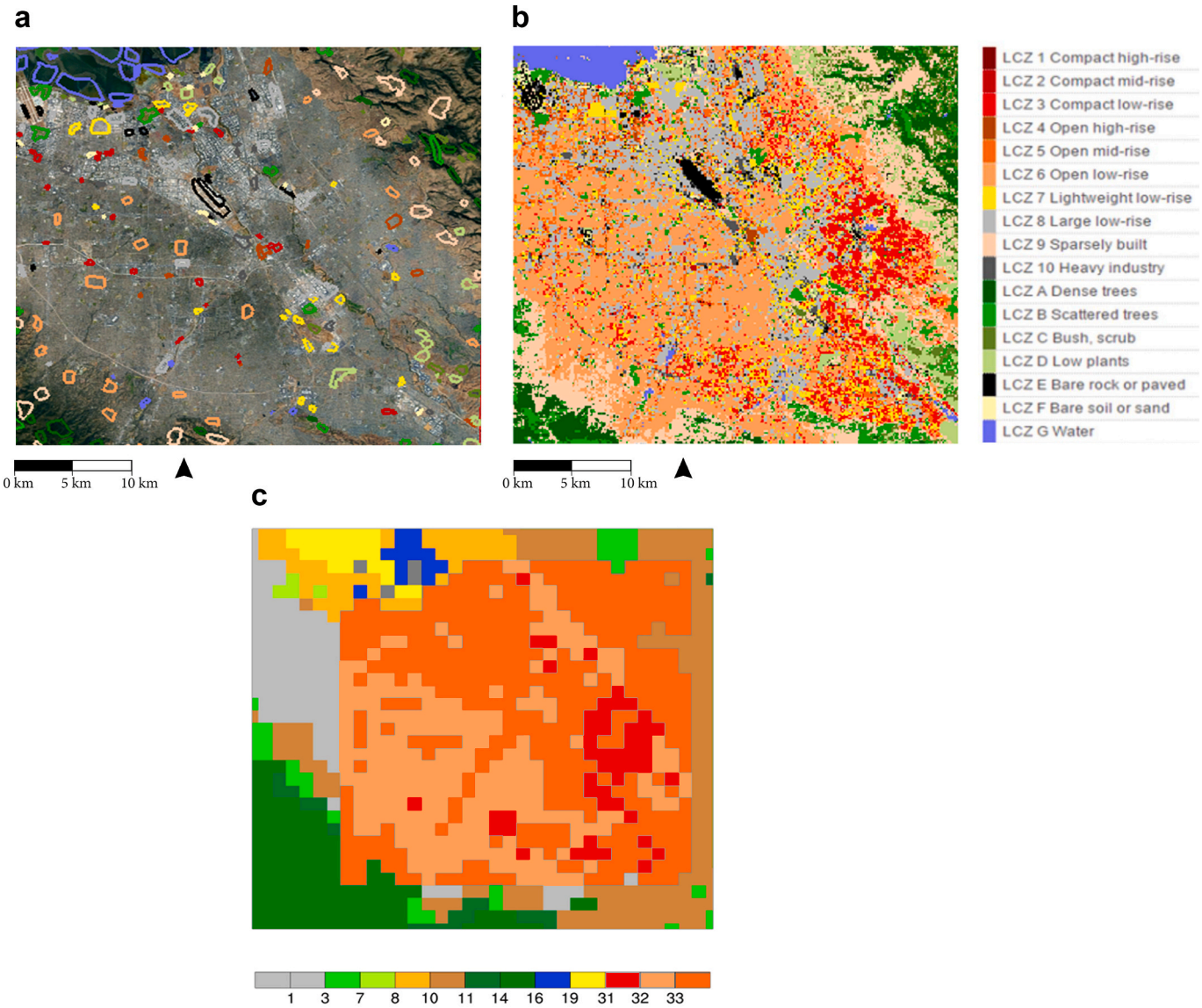

Fig. 5. WUDAPT Level-0 Local Climate Zones (LCZs, defined at right) for the area of Fig. 2b, showing its: (a) training zones, (b) final 100-m grid distribution, and (c) 1 km aggregated input for urbanized WRF. Also shown are the sites of the: San Jose Airport (SJA), San Jose State University (SJSU), and ENVI-met study area (within a portion of the WRF grid cell, indicated by black box).

Table 3
Accuracy Matrix for San Jose WUDAPT Level 0 training areas, with known (vertical axis) vs. predicted (horizontal axis) test-class frequencies. The uWRF building classes 31 to 33 defined in Table 2a are comprised of the following WUDAPT urban LCZ classes: 3 is in 31; 6 is in 32; and 4, 5, 7, 8, and 10 are in 33.

Defined		Predicted	2	3	4	5	6	7	8	9	10	A	B	C	D	E	F	G	Σ Pixels	User's Accuracy (%)
	LCZ 2	Compact mid-rise	**0**	0	0	2	0	0	0	0	0	0	0	0	0	1	0	0	3	0
	LCZ 3	Compact low-rise	1	**1**	0	0	24	0	1	0	0	0	0	0	0	0	0	0	27	4
	LCZ 4	Open high-rise	0	0	**8**	0	0	0	1	0	0	0	0	0	0	0	0	0	9	89
	LCZ 5	Open mid-rise	1	0	2	**3**	0	0	0	0	1	0	0	0	0	0	0	0	7	43
	LCZ 6	Open low-rise	0	0	0	3	**52**	0	1	0	2	0	1	0	0	0	0	0	59	88
	LCZ 7	Lightweight low-rise	1	0	0	0	10	**9**	4	0	4	0	0	0	0	0	0	0	28	32
	LCZ 8	Large low-rise	5	3	6	4	1	0	**12**	0	8	0	0	0	0	1	0	0	40	30
	LCZ 9	Sparsely built	0	0	0	0	2	0	0	**7**	0	1	2	2	5	0	1	0	20	35
	LCZ 10	Heavy industry	7	1	0	0	0	0	1	0	**7**	0	0	0	0	0	1	0	17	41
	LCZ A	Dense trees	0	0	0	0	0	0	0	0	0	**13**	0	0	0	0	0	0	13	100
	LCZ B	Scattered trees	0	0	0	0	0	0	0	0	1	1	**12**	0	1	0	0	0	15	80
	LCZ C	Bush, scrub	0	0	0	0	0	0	0	0	0	1	0	**0**	1	0	0	0	2	0
	LCZ D	Low plants	0	0	0	0	0	0	0	0	0	0	0	0	**6**	0	0	0	6	100
	LCZ E	Bare rock or paved	3	0	0	0	0	0	1	0	0	0	0	0	0	**28**	4	0	36	78
	LCZ F	Bare soil or sand	0	0	0	0	0	0	0	0	0	0	0	0	0	0	**5**	0	5	100
	LCZ G	Water	0	0	0	0	0	0	0	0	0	0	0	0	0	0	0	**36**	36	100
		Σ Pixels	*18*	*5*	*16*	*12*	*89*	*9*	*21*	*7*	*23*	*16*	*15*	*2*	*13*	*30*	*11*	*36*		
		Producer's Accuracy (%)	*0*	*20*	*50*	*25*	*58*	*100*	*57*	*100*	*30*	*81*	*80*	*0*	*46*	*93*	*45*	*100*		
			Overall Accuracy: 62%																	
			Kappa: 0.57																	

m to allow for large vehicles.

The distribution of impacted areas for each strategy is shown in Fig. 4, a manually digitized satellite image from Google Earth Pro and illustrated by Adobe Photoshop to emphasize modeled features. This process removed vehicles, conformed similar ground surfaces to a single color, and gave vegetation a common graphic convention for easier legibility. The accompanying aerial perspectival graphic is a screen capture from ENVI-met.

The default ENVI-met database provided values of the following ground and building material thermodynamic properties: α, ϵ, k, specific heat (c), absorptivity (a), and density (ρ). These values (not shown) are independent of those used in the WRF simulations. Additional building materials were added to the database to account for some SJ residential and commercial buildings, e.g., wood siding, asphalt roofing shingles, and lime plaster stucco.

Tree- and shrub-type and distributions were visually inferred from Google Earth Pro imagery and the ENVI-met V4.3.0 default 3-D plant library. Emphasis was on tree height, canopy shape, and deciduous vs. coniferous; species specific determinations were not necessary for this study. Default values for α and foliage solar transmissivity (τ) varied between 0.18 and 0.3 for deciduous and between zero and 0.12 for coniferous trees. Results were obtained for 20 ENVI-met simulations, each with only uWRF meteorological input. Five scenarios (existing LU/LC, three sub-strategies, and a combined strategy) were each run for the extreme (1 September) and typical (9 July) daytime and nighttime periods. Resulting street canyon (indoor areas thus excluded) 1 m level changes (ΔT) were defined as a mitigated minus an original T-value.

Daytime and nighttime simulations started at 0700 and 1500 LST, respectively, and were run for 9 h. Results from the first 5 h of each simulation were discarded, as this was considered a spin up period. This spin up is longer than the 1 h typically used for ENVI-met [20]. The model was run on a desktop computer with an Intel Core i7-3770K CPU clocked at 4.1 GHz and with 32 GB of RAM. One hour of simulation time with a model-prescribed time step of 10 s required about 6 h of clock time.

3. Results and discussion

3.1. WUDAPT level 0 distribution

The WUDAPT LU/LC training map (Fig. 5a) shows the manually digitized initial training areas used to run the LCZ classification process in SAGA. When tested on the remaining training areas, Table 3 shows it yielded an overall accuracy of 62% and a Cohen kappa coefficient of only 57%, as the latter corrects for chance agreements. These results are generally consistent with those from similar efforts [10], e.g., from Hong Kong with its homogenous urban morphology of high-rise buildings [47]. The SJ non-urban LCZ classes A, D, F, and G showed perfect accuracy (right most column of results). Urban classes with 80–90% accuracies include LCZs 4 and 6. Urban LCZs 2 and 3 had the lowest accuracy, but they only contained 3 and 27 training areas, respectively. Poor accuracies (thus with large off diagonal values) exist between some low-rise classes, i.e., compact vs. open low-rise (24 of 27 areas) and open vs. lightweight (10 of 28). Poor accuracies are also seen between compact mid-rise versus heavy industry (7 of 17) and between heavy industry and lightweight low-rise (7 of 17) and large low-rise (8 of 40).

When the classification was applied to the entire study area, the resulting 100 m distribution (Fig. 5b) shows LCZ 6 (defined in Table 3) as the most common. LCZ 8 areas are mainly in north SJ and along east-west corridors that parallel its main avenues, while LCZ 3 areas with little or no green space exist mainly in east SJ. The scattered LCZ 7 areas are mobile homes, mainly constructed of light-weight materials such as lumber. LCZ 9 areas exists near the hills on either side of the valley, while LCZ 4 areas are mainly near downtown SJ. LCZ E areas correspond to large parking lots near the SJA and Moffett Field airports.

Aggregation of the 100 m LCZ areas (Fig. 5b) into the gridded 1-km LU/LC distribution for the *Urban-WRF* simulation (Fig. 5c) shows that most of the SLUCM domain is comprised of urban Classes 31 , 32 and 33 (defined in Table 3). Note that the last three urban types of Class 33 are 50% of the six LCZs with the poor accuracy values discussed above, and thus their grouping negates their errors. Class 32 is dominant in the southwestern part of the domain and 33 in its northeastern half. The SJA

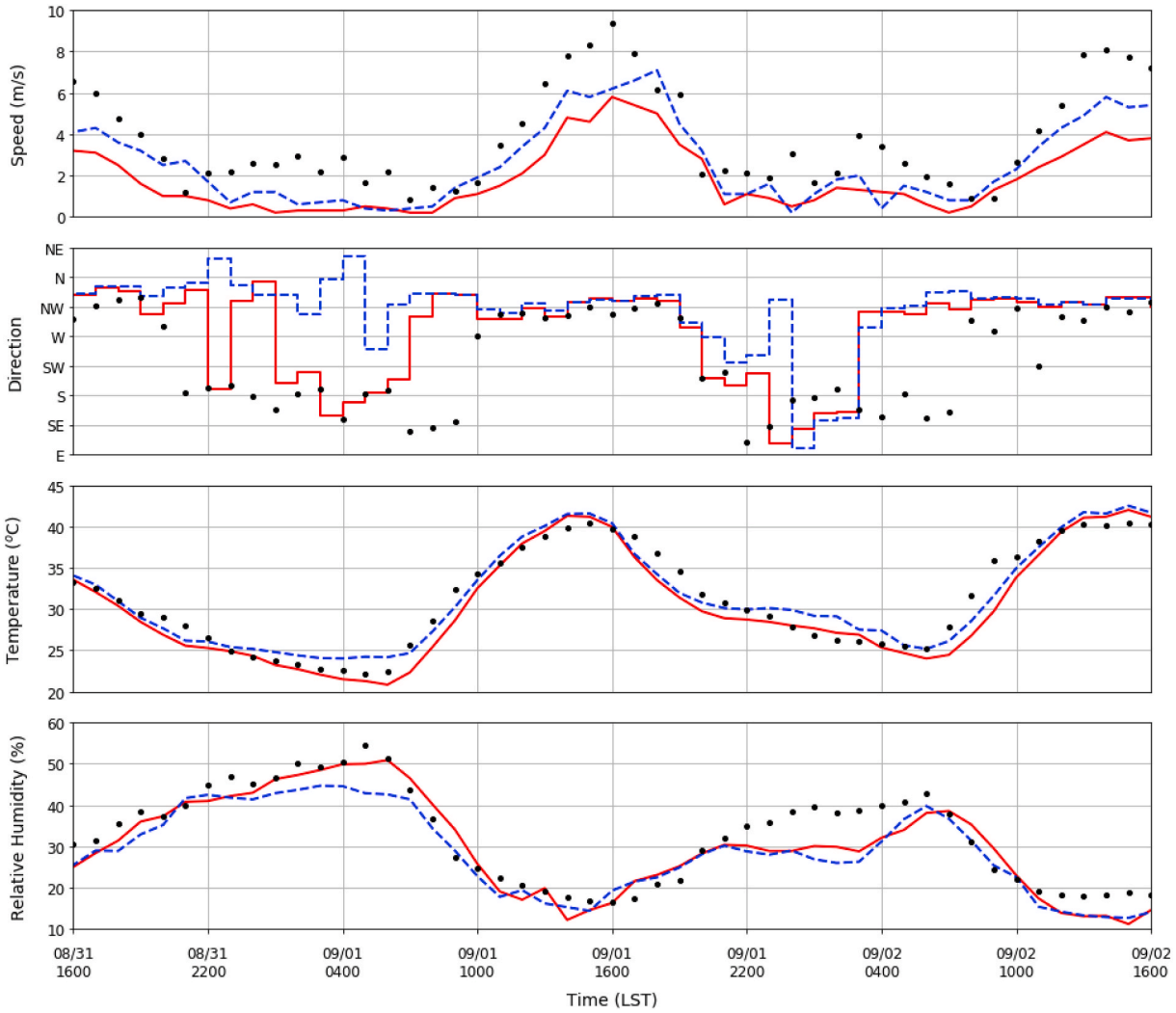

Fig. 6. Observed hourly meteorological conditions (dots) at SJSU, as well as corresponding *Urban-WRF* (red line) and *Default-WRF* (blue line) simulation results at the closest grid point to the observations. Data start on 31 August at 1600 LST, and periods of most interest are 1200–1500 LST and 2000–2300 LST on 1 September. (For interpretation of the references to color in this figure legend, the reader is referred to the Web version of this article.)

and SJSU meteorological observation sites are in different Class 32 WRF grid cells, while the ENVI-met study area is in a Class 31 cell.

3.2. WRF results

Simulated diurnal patterns of 2-m level T from both the *Urban-* and *Default-WRF* runs, as compared to the SJSU observations during the extreme temperature period (Fig. 6), show generally good agreements (within 1–2 °C), especially for the *Urban-WRF* run. Both the daytime peaks (of about 41 °C) during the 1 September extreme day and its minima (still high at about 25 °C) during the following night were particularly well simulated. Relative humidity (RH) was also well simulated (within 5%) by both models throughout most of the period; values were (as expected) high at night and low during the day. One exception is with its nighttime values preceding the extreme T period, when only *Urban-WRF* performed well. Another is during the night after the extreme T, when both performed not so well (10% errors). The current high daytime T-values, followed by relatively high nighttime RH-values, produce extreme human heat stresses, as nocturnal recovery cannot occur.

Simulated 10-m level V values show under-predictions of about 2 m s^{-1} during both the expected higher-speed daytime and low-speed nighttime periods. The peak-T period shows some of the largest under-predictions, and *Default-WRF* generally shows somewhat smaller errors. This systematic underprediction probably results as the SJSU observations are taken atop an eight-story building, as V generally increases with height. The most difficult parameter to simulate is dd, given its observed abrupt shifts during the low speed nights before and after the daytime extreme T. This shift is typical of summer conditions in the SCV and it results from a change from the predominantly up valley northwesterly daytime winds to the predominantly down valley southerly nighttime flows. While both models perform well during the uniform flow on the heatwave day, *Urban-WRF* was somewhat better in capturing the nighttime shifts before and after that day.

While similar simulated T and RH accuracies for both models are seen at the SJA site (Fig. 7), *Urban-WRF* better simulated the peak V on the extreme T day. Both models also better simulated the nocturnal low V periods before and after the extreme T day. Both again capture the dd-values during the uniform northwesterly flow on the extreme T day. *Default-WRF* performs better (but not outstandingly) with the more constant dd values during the preceding night, but neither does well during the night following the extreme T, when dd again changes rapidly.

While only the SJA meteorological observations are used as input to some ENVI-met simulations, the above analysis indicates that *Urban-WRF* was generally better than *Default-WRF* in reproducing both the SJA and SJSU observations, specifically in its ability to capture the complex nighttime SJSU wind shifts during the night following the daytime T-extremes. As SJA and SJSU are located about 7.3 and 2.5 km northeast, respectively, of the *Urban-WRF* grid cell closest to the ENVI-met study

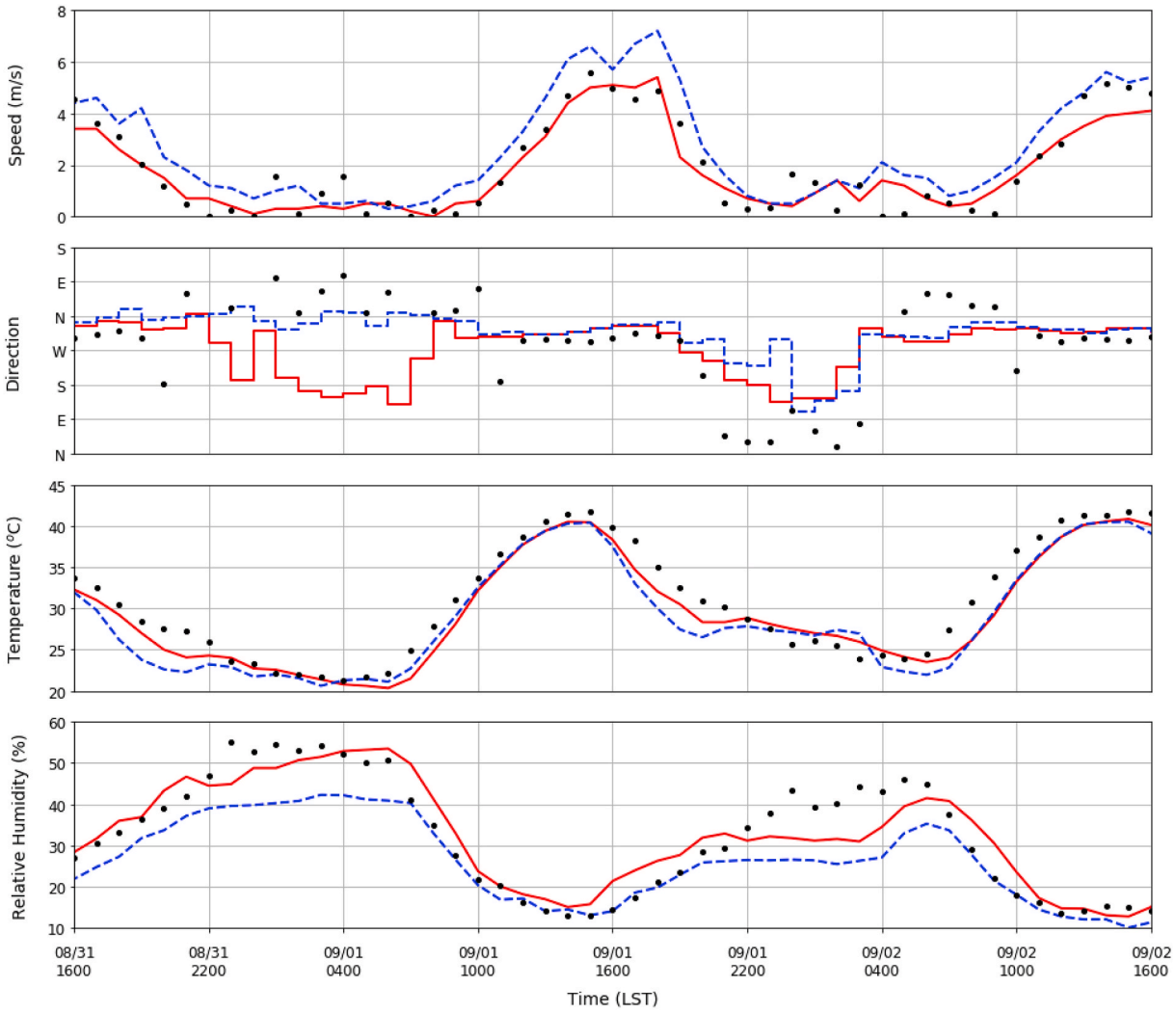

Fig. 7. Same as Fig. 6, but for the *San Jose Airport (SJA)* observational site.

area (Fig. 3c), it is expected to show a similar accuracy at that cell, which does not contain any meteorological observations.

The observed or WRF meteorological output values used for each ENVI-met simulation are given in Table 1. Constants across all simulations (not shown) include z_o and cloud cover, set to 0.1 m and zero, respectively. As incoming solar radiation R is not measured at SJA or OIA, the ENVI-met default value of unity was used for the solar τ for the *SJA-Airport* simulations, while the *Default-WRF* and *Urban-WRF* values of 0.89–0.92 were derived from their calculated R-values. An assumed constant (in time and height) upwind BC of 1.5 m s^{-1} wind speed (as discussed above) was used for all ENVI-met simulations.

The remaining Table 1 inputs to ENVI-met allow it to capture meteorological features appropriate to the typical and extreme days. NWS surface weather maps (not shown) on the former day indicate

Table 4a
ENVI-met domain-wide average simulated 1-m level street-canyon air temperatures (T) obtained from urbanized WRF inputs for a variety of mitigation strategies on both the extreme (1 September) and typical (9 July) days at 1500 and 2300 LST. Values are means (μ) and standard deviations (σ).

T (μ ± σ, °C)				
Simulation / Mitigation strategy	Extreme Day 1500 LST	Extreme Day 2300 LST	Typical Day 1500 LST	Typical Day 2300 LST
Existing	39.21 ± 0.71	28.85 ± 0.32	30.98 ± 0.66	21.41 ± 0.42
Roof albedo	39.21 ± 0.71	28.85 ± 0.32	30.99 ± 0.66	21.41 ± 0.42
Solar shading	38.97 ± 0.71	28.82 ± 0.32	30.69 ± 0.66	21.46 ± 0.42
Vegetation	38.14 ± 0.77	28.62 ± 0.45	29.91 ± 0.65	21.38 ± 0.49
Combined	37.72 ± 0.78	28.51 ± 0.44	29.57 ± 0.60	21.38 ± 0.49

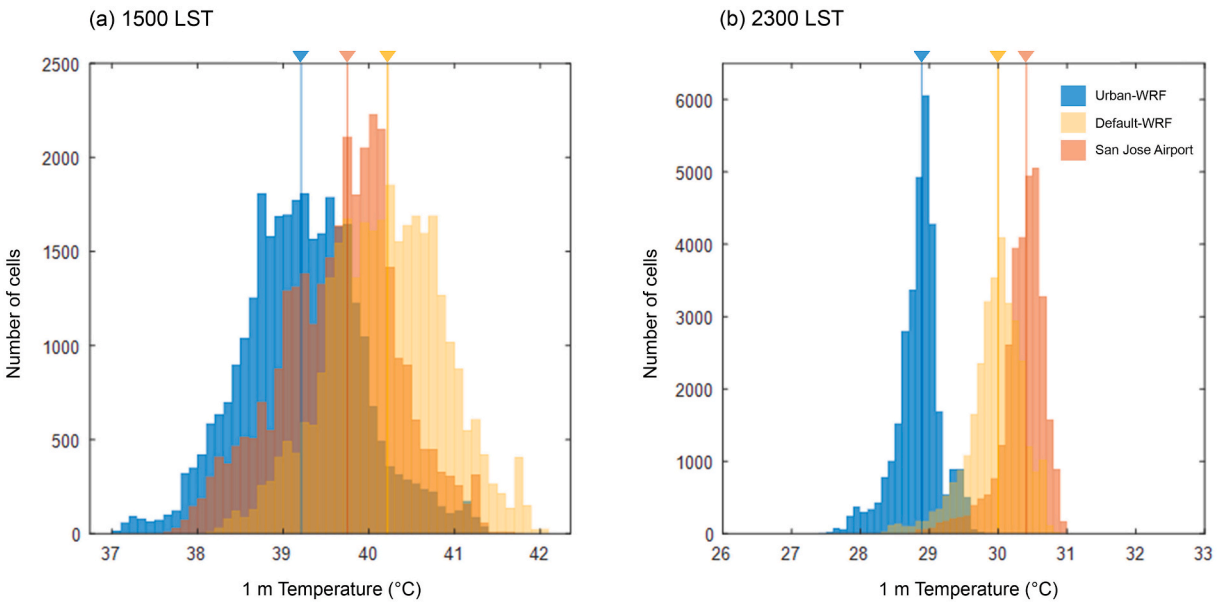

Fig. 8. Frequency distributions of ENVI-met 1-m level street canyon air temperatures (excluding building interior grid-points) for the existing LU/LC conditions on the extreme heat day of 1 September for the *Urban-WRF* (blue), *Default-WRF* (yellow), and *SJA* (orange) driven-simulations at (a) 1500 and (b) 2300 LST. Vertical lines and inverted colored arrow heads mark mean values; note different vertical and horizontal scales. (For interpretation of the references to color in this figure legend, the reader is referred to the Web version of this article.)

normal California summer conditions, as the pressure difference between the offshore Pacific high and California thermal low created a cool regional onshore flow. Conditions on 1 September were those of a typical (fall) Indian Summer heat wave, as part of the offshore high pressure moved inland and north of California, and thus created a hot regional offshore flow.

The constant with time (observed or modeled) wind direction BCs for each simulation (Table 1) represent those at the end of the daytime or nighttime simulations, i.e., 1500 and 2300 LST, respectively, the hours investigated in depth. Day-night variations differ, as the typical day shows a northwesterly flow down the SCV during both daytime and nighttime hours. The extreme day, however, shows a shift to a generally southwesterly up-valley flow sometime during the afternoon. Neither of the above daytime directions reflect the onshore or offshore regional flows discussed above, as the SCV is frequently sheltered from such flows, especially with low wind speeds when it produces its own flows.

As PBL depth (H) is not observed at SJA, and only at 12 h intervals at OAI, the ENVI-met default value of 2500 m was used in all *SJA-Airport* simulations (Table 1). Simulated daytime H values at 1500 LST are about 510 m, while the default value for the *SJA-Airport* cases is thus excessively large. The same pattern is true for the nighttime (2300 LST) simulated values, all lower by a factor of about 16 from their daytime values, reflecting the normal rapid post-sunset collapse of PBL height. The near uniform simulated H values on both the days do not imply that the regionally dominated flows below H are similar on both days, as discussed in the previous paragraph. The only impacts of H in a 3-D ENVI-met simulation is from its associated 1500 and 2300 LST q-values, which only indirectly impact the simulated T and V fields. The low observed *SJA-Airport* q values at its higher H reflect the normal decrease of q with altitude. The H values do, however, directly impact the 1-D ENVI-met solutions that provide its inflow BCs.

The 2 m level hourly T and RH values nudge the ENVI-met inflow BCs at every Δt, and the maximum and minimum values in Table 1 are those during each daytime and nighttime simulation, respectively. These occur at the end of each simulation period because of how the periods were selected. These values reflect the different conditions on the two simulation days, e.g., on the extreme day, the daytime and nighttime values are about 10 and 7 °C warmer, respectively, than on the typical day. The values across all three data sources for the extreme day are similar in magnitude during both daytime and nighttime hours. The corresponding RH values on the typical day are higher by about 10–20% than on the extreme day, consistent with its lower T-values, and not necessarily of a higher q-value. These T and RH input values do reflect the regional hot and cool air masses that impacted T within the SCV on the extreme and typical days, respectively.

While the input data for the three extreme day simulations in Table 1 do not show large differences, the combination of the individual differences does produce significant variations between the three ENVI-met results, as well as between the extreme and typical days. The next sections discuss these differences.

3.3. ENVI-met temperatures

Fig. 8 shows three frequency distributions of 1 m level (all subsequent results will also be at this level) ENVI-met simulated street-canyon T-values (building interior grid points thus not included in this or the following results) at two times during the extreme T day of 1 September. The values are from ENVI-met simulations driven by meteorological data from the *Urban-WRF* output, *Default-WRF* output, or *San Jose Airport* observations. Similar comparative results are not shown for the typical day, as only *Urban-WRF* simulations were carried out for 9 July. Histograms at 1500 LST (Fig. 8a) show all three distributions with a similar range of T-values (about 3 °C) and a similar peak number of cells (about 2000 ± 250). The *Urban-WRF* mean value (μ) of 39.2 °C (Table 4a), however, is cooler than the *Default-WRF* value, while that from *SJA* is in between the two; the difference in both comparisons is about 0.5 °C. The corresponding 2300 LST mean T values (Fig. 8b) are lower (as expected) by about 10 °C and their ranges are also narrower (2 °C). Peak cell-numbers are thus higher (4000–6000), also with larger differences between the cell number peaks. The *Urban-WRF* μ (28.9 °C, Table 4a) is again the lowest, but the *SJA* value is now higher than the *Default-WRF* mean. The difference between the lowest two values has thus increased to about 1 °C, while that between the top two is still about 0.5 °C.

Table 4a also gives standard deviation (σ) values for all four distributions, and the results show that the extreme daytime period σ values are always larger than the corresponding typical period values, with the reverse true for the nighttime period. All daytime σ values are likewise

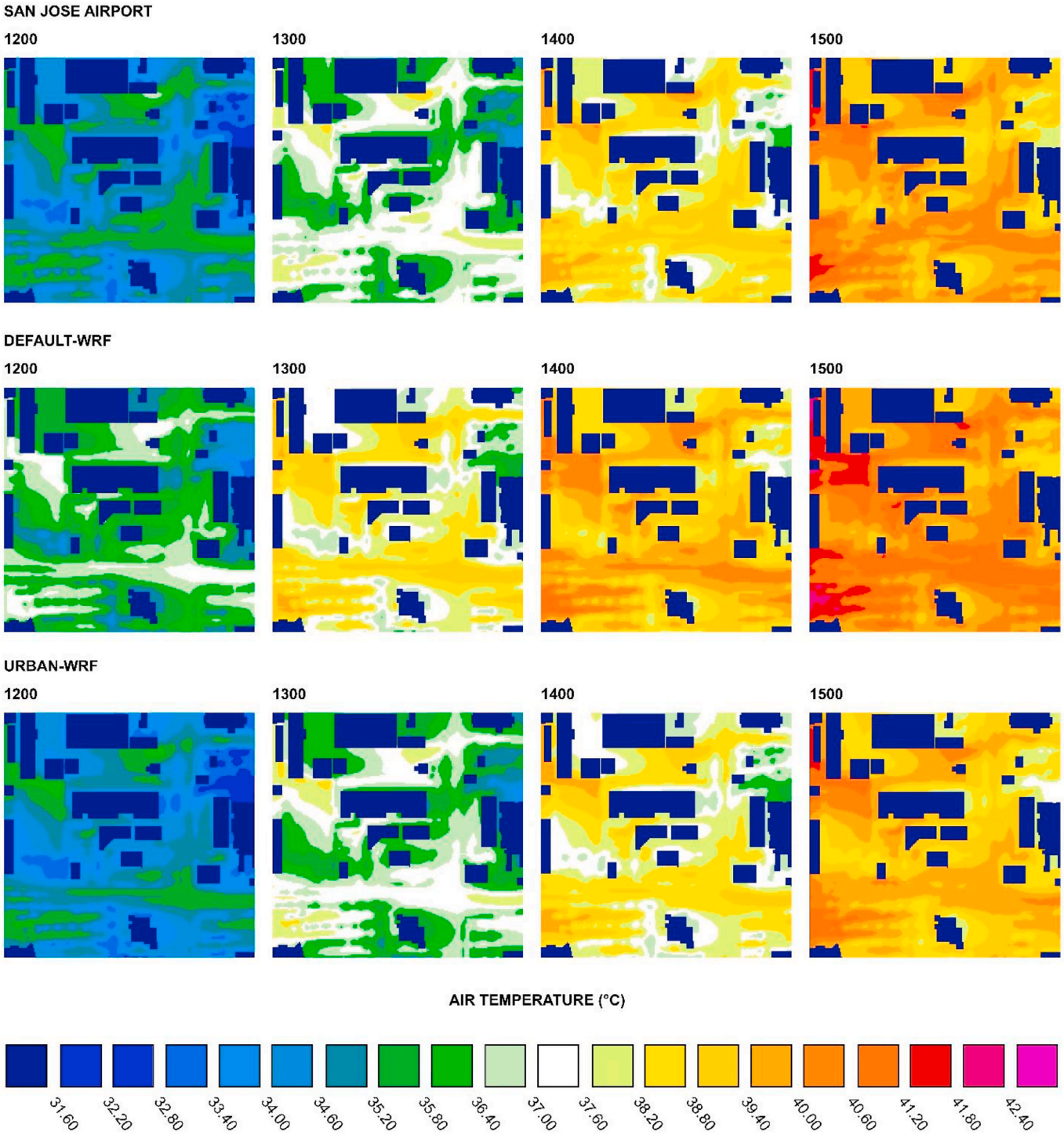

Fig. 9. Evolution of hourly (1200–1500 LST) ENVI-met 1-m level street canyon air temperatures in the study area on the extreme heat day of 1 September for the *SJA* (upper), *Default-WRF (middle)*, and *Urban-WRF* (lower) driven-simulations under existing LU/LC conditions; rooftops shown in black.

larger than all corresponding nighttime values during both periods.

The time evolution of the hourly 1200–1500 LST spatial distribution of ENVI-met street-canyon 1 m level T values on the extreme temperature day is shown in Fig. 9, as driven by each of the three input meteorological datasets. The evolution of the *Urban-WRF* values resembles that from the *SJA* case, while that of the *Default-WRF* case warms faster by an hour, consistent with its warmest values in Fig. 8a. The largest range of temperature values occuring across the three cases together (6 °C) occurs at 1200 LST, with the smallest (5 °C) at 1400 LST. The *Default-WRF* and *SJA* cases show the largest temporal variations (10 °C), while *Urban-WRF* has the smallest (9 °C).

The corresponding 2000–2300 LST hourly distributions (Fig. 10) show that the evolution of the *Default-WRF* values is now closer to that of the *SJA* case, while the *Urban-WRF* values now cool faster by 2 h, consistent with its considerably cooler values in Fig. 8b. The spatial differences between the cases was largest (but only 4 °C) at 2100 LST

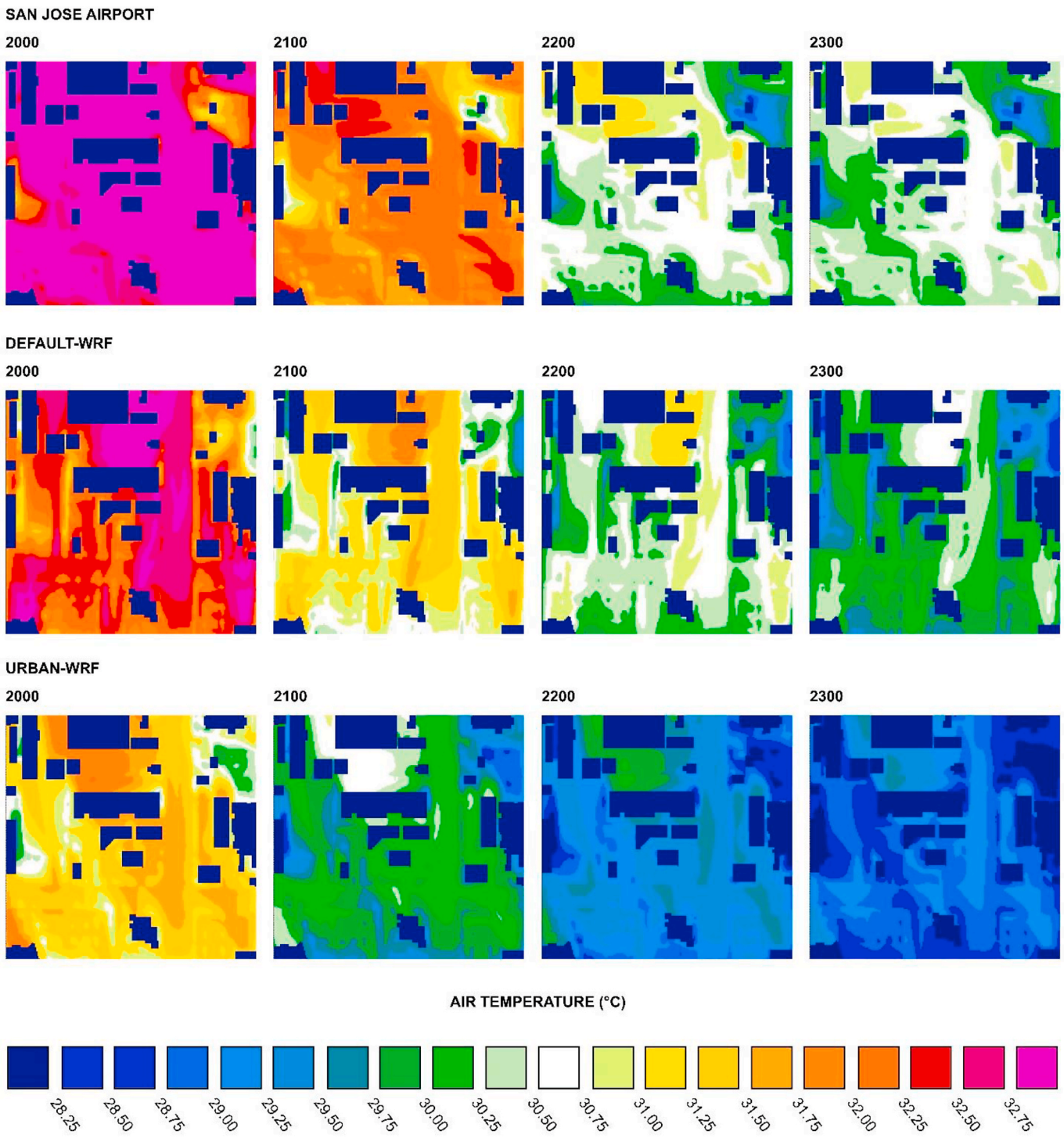

Fig. 10. Same as Fig. 9, but for 2000–2300 LST.

and smallest (3 °C) at 2300 LST. The *Default-WRF* case has the largest variations across all 4 h (4.5 °C), while *Urban-WRF* has the smallest (3.8 °C).

In summary, the Urban-WRF simulation warmed to a lower maximum due to the higher thermal inertia of its scheme. The lower maximum resulted in cooler nocturnal temperatures throughout the nighttime simulation. The choice of input meteorological data set thus impacts ENVI-met T results. Many of the hourly patterns show detailed inter- and intra- street patterns that could be verified in future urban microscale studies containing in-domain observational sites.

3.4. Mitigation results

The ENVI-met histograms in Fig. 11 show mitigated T-values, but only those driven by meteorological data from *Urban-WRF* and only for both daytime periods. Nighttime changes were smaller, as the current mitigation strategies were designed to more highly impact extreme daytime values. Results are shown for all five scenarios: existing conditions, three mitigation cases, and combined case. Extreme day values (Fig. 11a) show all three sub-scenarios with similar peak cell frequencies, while the combined strategy has a somewhat higher peak (1100 vs 900). Difference between the μ values of the three scenarios is

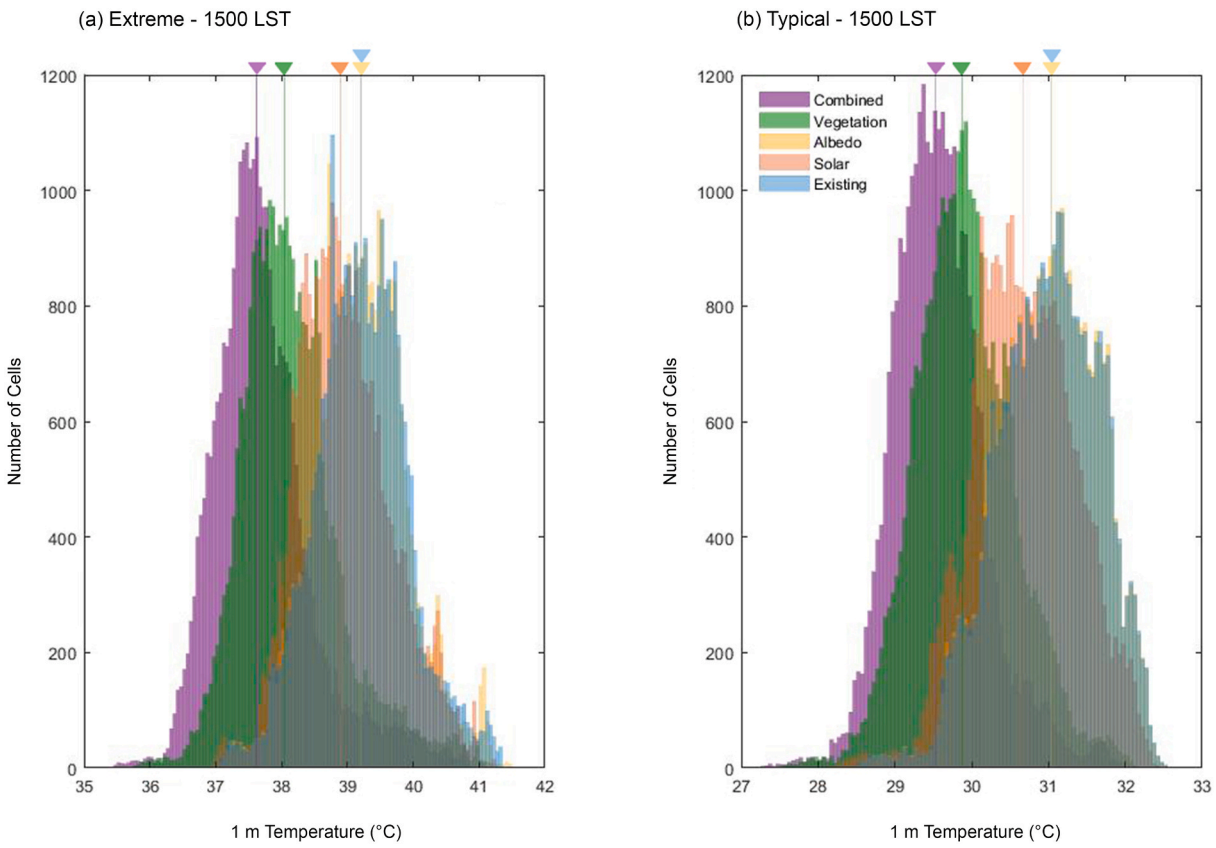

Fig. 11. Frequency distributions of mitigated 1-m level ENVI-met street canyon (excluding interior building grid-points) air temperatures at 1500 LST on the: (a) extreme heat day of 1 September and (b) typical day of 9 July. Results shown for white roof albedo (yellow), solar shading (orange), and vegetation (green) mitigation strategies, as well as for both their combined effects (purple) and pre-existing LU/LC conditions (blue). Note the different horizontal scales, and that each simulation is driven by *Urban-WRF* meteorological output and that inverted colored arrow heads mark mean values. (For interpretation of the references to color in this figure legend, the reader is referred to the Web version of this article.)

about 1.1 °C, with the vegetation strategy (μ of 38.1 °C) as the coolest, followed by the solar shade strategy, which aligns with previous studies [61]. The rooftop albedo and existing condition scenarios have near identical values, indicative of its insignificant impact on street canyon values. The combined strategy μ, of course, is coolest. The typical day histogram (Fig. 11b) shows lower T values (by about 8 °C), as expected, but their means are ranked in the same order as on the extreme day.

To focus on warming and cooling impacts associated with each mitigation strategy, the daytime ENVI-met results for the two days of Fig. 11 are shown in Fig. 12 as histograms of ΔT-values, defined as a mitigated T minus its unmitigated value. Note that μ values are not shown, as both distributions are somewhat noisy. The maximum number of grid cells for the roof albedo and solar shading mitigations on the extreme day are about 20 000 and 7 000, respectively, while for the typical day they are about 20 000 and 10 000, respectively. For legibility purposes, the vertical axis extends only to 6000 occurrences.

The extreme day results (Fig. 12a) show greening producing the largest impacts, with cooling to about −3.5 °C, followed by solar shading to about −1.6 °C. The white roof albedo strategy, however, produces a few cases of weak warming to about 1.0 °C, but with many values close to zero. The combined mitigation impacts, of course, show the greatest cooling, with values up to about −3.7 °C. The corresponding typical days histogram (Fig. 12b) shows similar results as compared to the extreme day, but with generally smaller maximum changes.

These similarities are highlighted in Table 4b, which summarizes the daytime mitigation impacts on canyon level T values on both days. The results show that, as sub-mitigation μ values increase, so do their corresponding σ values. Extreme day μ values are always larger than the corresponding typical values, while ranking their σ values does not show a consistent pattern. Roof top albedo mean impacts are insignificant on both days (consistent with Fig. 12) while vegetation again shows the largest values. Shading and vegetative μ values are both slightly larger on the typical day, as is its simple linear summation (L in table) of the three sub-mitigation contributions (−1.38 vs. −1.31 °C). It is thus somewhat surprising, given that the μ value for the combined mitigation simulations (C in table) is larger on the extreme day (−1.49 vs.-1.42 °C). This could be explained by its significantly larger (0.18 and 0.04 °C) nonlinear interaction term (NL in table), with the complex causes of this effect beyond the scope of the current effort.

The spatial distributions of the ENVI-met 1 m level street canyon cooling impacts (ΔT) at 1500 LST for both daytime cases are shown in Fig. 13. For the extreme day (upper row), the vegetation strategy again shows the largest cooling (up to −3.5 °C). Solar shading showed a smaller impact (−1.6 °C), but with some surprising warming (0.9 °C). The high albedo rooftops showed mostly insignificant impacts (±0.1 °C, consistent with Table 4b), but with a few small areas of cooling (−0.3 °C) and an even larger warming (1.0 °C). The combined strategy again thus strongly resembled the vegetative case, but with a slightly larger maximum cooling (−3.7 °C), due to linear and nonlinear contributions from the other two strategies. The corresponding overall distributions and maximum cooling magnitudes for the typical daytime cases (lower row, Fig. 13) are similar to the extreme day values. An exception is the almost total lack of warming areas for the solar shading and high roof albedo cases. These warming areas are weak and/or small in extent; their maxima are 0.04 and 0.32 °C, respectively.

In summary, these hourly T mitigation patterns again show detailed intra- and inter- street variations that thus could be useful in the planning and evaluation of future microscale urban climate studies under

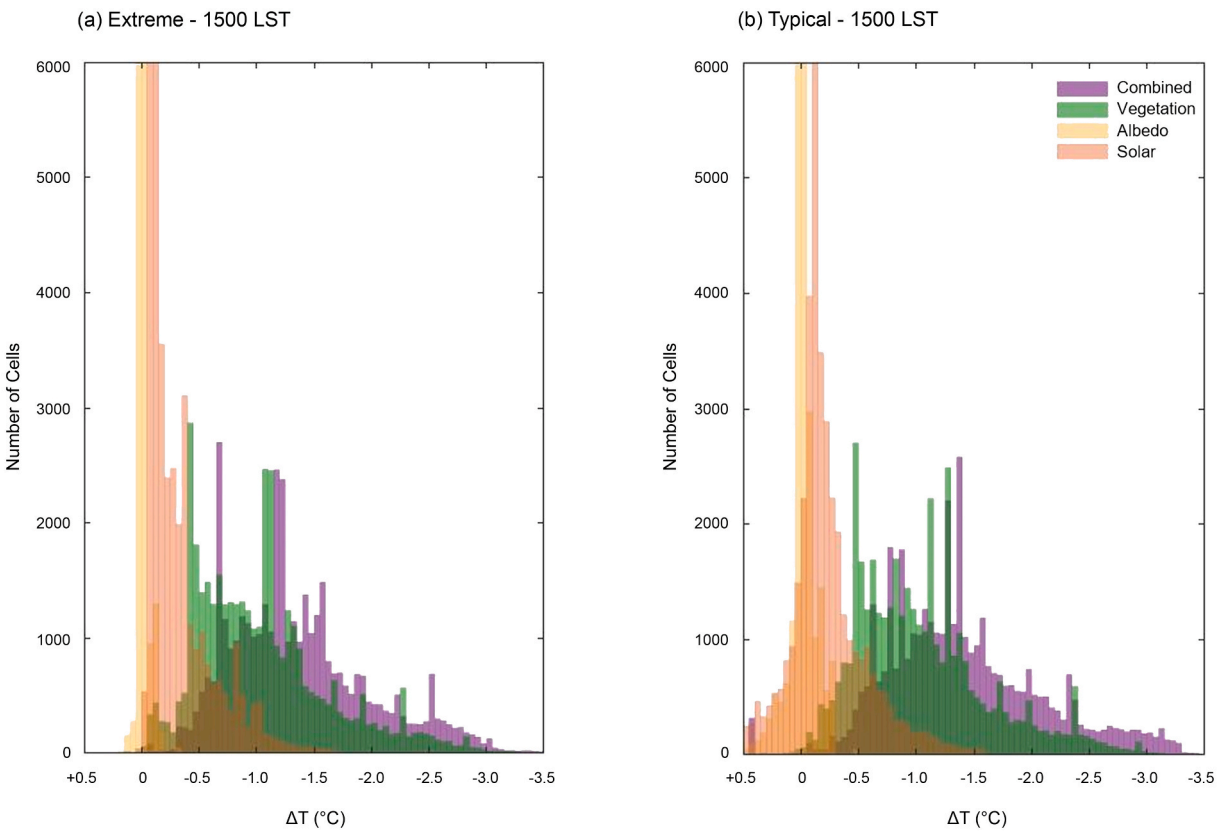

Fig. 12. Same as Fig. 11, but for the resulting mitigated temperature differences ΔTs (mitigated minus pre-existing values). Note that the maximum number of grid cells for the roof albedo and solar shading mitigations on the extreme day are about 20 000 and 7 000, respecttively, while for the typical day they are about 20 000 and 10 000, respectively. For legibility purposes, the vertical axis extends only to 6000.

extreme and typical conditions [60]. While the reductions in mean daytime T of 3–4 °C across the study area may seem small, epidemiological studies have shown that mortality rates increase by 1–3% for every 1 °C increase in average maximum T [28].

4. Conclusion

An obstacle to the evaluation of strategies to mitigate extreme urban temperatures by numerical microscale models is frequently the lack of on-site meteorological data. The current study thus reports on an innovative method that used the WUDAPT Level 0 methodology to generate a Local Climate Zone (LCZ) land-use/landcover (LU/LC) distribution as input to the WRF weather prediction model. Its meteorological output was then used to generate inputs for the ENVI-met microscale planning model to produce 1-m level building-scale street canyon temperature fields. The ENVI-met study area was a 300 m square near downtown San Jose, CA, and the day of interest was then the hottest in California history. The model was used to simulate a variety of daytime and nighttime temperature-mitigation strategies at a 1.5 m grid for this day and for a second more typical summer day.

The source of the meteorological data for a given ENVI-met simulation was either the urbanized version of WRF; default version of WRF; or observations at the closest NWS site, historically the most commonly source. WRF output at its grid point closest to the study area provided time-varying lateral boundary conditions for the ENVI-met simulations, run on a 1.5 m cubic grid. The temperature mitigation strategy was comprised of three sub-strategies that either increased surface vegetation, rooftop albedo, or architectural shade elements. The 20 ENVI-met mitigation simulations each used only data from urbanized WRF, as it provided the most accurate data. The five mitigation scenarios (existing LU/LC, three sub-strategies, and a combined strategy) were carried out for the daytime and nighttime periods on the extreme and typical days. Resulting street canyon 1 m level changes (ΔT) were defined as a mitigated minus an original unmitigated value.

Results showed that the WUDAPT Level 0 training LU/LC areas demonstrated a typically high ability to classify test areas with known land cover types. The scheme was thus applied with a 100 m grid resolution to the entire WRF computational domain, with the results finally aggregated to the WRF grid. WRF test simulations showed that both versions accurately reproduced the diurnal cycle of 2 m temperature and relative humidity on both days at two observational sites near the ENVI-met study area. While both, however, overestimated the low daytime and nighttime wind speeds at the NWS airport site on the extreme day, they accurately reproduced the near constant wind directions during the daytime hours at both sites. Only urbanized WRF, however, captured the extreme nighttime wind shift at the non-NWS site, the one closest to the ENVI-met study area.

All mitigation strategies had only negligible impacts on ENVI-met simulated nighttime 1 m level canyon air temperatures. Increased vegetation, however, was the most effective daytime strategy on both days as its implementation effected the largest fraction of the ENVI-met domain, like in the results of [48]. The maximum cooling across the domain on the two days was −3.5 and −3.3 °C, respectively. While increased rooftop albedos produced near negligible cooling impacts, increased solar shading produced corresponding maxima of −1.6 and −1.7 °C, respectively. The reductions in mean daytime temperatures of 3–4 °C across the study area may seem small, but epidemiological studies have shown that mortality rates increase by 1–3% for every 1 °C increase in average maximum temperature.

One unanticipated result was formation of areas of daytime warming with the roof-top albedo and solar shading strategies on the extreme day, with maximum values of 1.0 and 0.9 °C, respectively. Corresponding typical day values, however, were only 0.32 and 0.04 °C, respectively. Another unanticipated result was that, while the simple linear

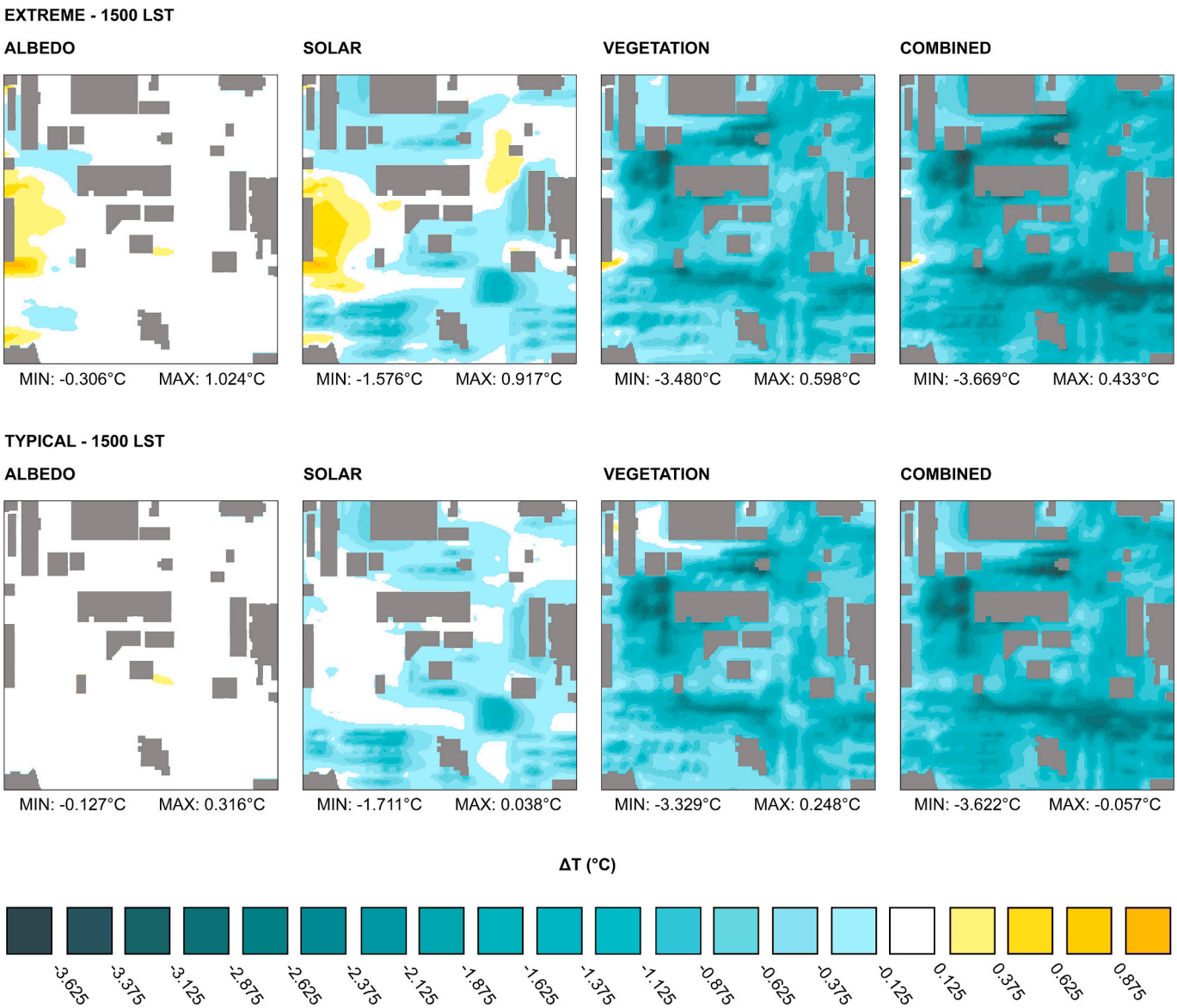

Fig. 13. ENVI-met 1-m level street canyon (excluding building interior grid points, shown in grey) temperature-differences (ΔT, defined as mitigated minus previously existing value) at 1500 LST on the extreme heat wave (1 September, upper) and typical (9 July, lower) days. Results show each of the three strategies separately and combined, and where each simulation is driven by *Urban-WRF* meteorological output.

summation of the three sub-mitigation cooling value was larger on the typical than extreme day (−1.4 vs. −1.3 °C), the combined mitigation cooling was larger on the extreme day (−1.5 vs.-1.4 °C). This reversal could be explained by the larger (0.18 vs. 0.04 °C) nonlinear interaction on the extreme day.

This study is a contribution to the field, as it demonstrates a new method of overcoming the frequent lack of on-site meteorological data for use in the evaluation of strategies to mitigate real world extreme urban temperatures by use of numerical microscale CFD planning models. The new method uses output from a meso-scale urban weather model as input into the microscale model. This technique will aid in development of site-specific temperature and wind data to inform a wide variety of strategies proposed to mitigate extreme and typical day weather conditions. ENVI-met produced detailed intra- and inter-street temperature variations that would be useful in the evaluation of microscale urban climate mitigation studies in a wide variety of global climate types under changing climate conditions.

Future efforts should overcome some limitations of the current effort, e.g., use of new techniques for more detailed bottom-up building data inventories and use of more advanced multilevel urban parameterization schemes in WRF. Recent versions of ENVI-met allow for more advanced linkages between it and WRF, e.g., ever larger ENVI-met domains and nudging with wind speed and direction. Additional studies are also needed to understand two unanticipated results from the current study: weak warming with some daytime cooling strategies, as well non-linear interactions when a variety of mitigation strategies are modeled simultaneously. Various parametric studies should also be carried out with these improved tools to study a wide range of urban landscapes in a variety of climate zones under changing regional climates. These studies should also investigate more advanced thermal stress parameters, e.g., those that involve T, RH, and wind speed.

While the current white rooftop mitigation strategy produced only small 1.5 m level canyon level impacts on daytime and nighttime temperatures, it did produce significant above-roof and building-interior daytime cooling (not discussed in the paper), both important for building energy applications. The current microscale results provide more detailed spatial information than do meso-scale urban weather models. Such meso-scale models can only adjust a single composite urban value per grid cell and may only report a single mitigated temperature for that cell. These studies need to be careful not to mix canyon

Table 4b
Like Table 4a, but for temperature impacts (ΔT, mitigated minus existing values) and only at 1500 LST, where L is the linear sum of the individual strategies, C the impact from a simulation of the three together, NL the non-linear synergistic effect, and negligible (<0.01 °C) values of μ are denoted by ( )*.

ΔT-values (μ ± σ, °C)		
Simulation / Mitigation strategy	Extreme 1500 LST	Typical 1500 LST
Roof albedo (A)	* ± 0.11	* ± 0.13
Solar shading (S)	-0.24 ± 0.36	-0.30 ± 0.29
Vegetation (V)	-1.07 ± 0.60	-1.08 ± 0.60
Combined (C)	-1.49 ± 0.69	-1.42 ± 0.63
L = A+S+V	-1.31	-1.38
NL = C–L	0.18	0.04

and building-interior results, and thus not to overestimate simulated in-canyon cooling rates.

In summary, the current effort builds upon a range of previous microscale urban heat mitigation studies . It accomplishes this by the expansion of the range of tools available to carry out such studies.

Declaration of competing interest

The authors declare that they have no known competing financial interests or personal relationships that could have appeared to influence the work reported in this paper.

Acknowledgements

This research was partly funded by an internal grant from the University of California at Berkeley. Helpful insights into ENVI-met were provided by Helge Simon and Michael Bruse of ENVI-MET GmbH and by Patrick Conry of LANL.

References

[2] A. Albatayneh, D. Alterman, A.W. Page, B. Moghtaderi, Warming issues associated with the long-term simulation of housing using CFD analysis, Journal of Green Building 2 (11) (2016) 59–74.
[3] P. Alexander, G. Mills, Local climate classification and dublin's urban heat island, Atmosphere 5 (4) (2014) 755–774.
[4] F. Ali-Toudert, H. Mayer, Numerical study on the effects of aspect ratio and orientation of an urban street canyon on outdoor thermal comfort in hot and dry climate, Build. Environ. 41 (2) (2006) 94–108.
[6] J.J. Baik, S.B. Park, Urban flow and dispersion simulation using a CFD model coupled to a mesoscale model, Journal of Applied Meteorology and Climatology 48 (2009) 1667–1681.
[8] L. Bande, P. Manandhar, P. Marpu, M. Al Battah, in: Local Climate Zones definition in relation to ENVI-met in the city of Dubai, UAE, IOP Conference Series: Materials Science and Engineering, 829, 2020, 6pp.
[9] B. Bechtel, P. Alexander, J. Böhner, J. Ching, O. Conrad, J. Feddema, G. Mills, L. See, I. Stewart, Mapping local climate zones for a worldwide database of form and function of cities, International Journal of Geographic Information 4 (1) (2015) 199–219.
[10] B. Bechtel, P.J. Alexander, C. Beck, J. Böhner, O. Brousse, J. Ching, Y. Xu, Generating WUDAPT Level 0 data – current status of production and evaluation, Urban Climate 27 (2019) 24–45.
[11] S. Bhati, M. Mohan, WRF-uran canopy model evaluation for the assessment of heat island and thermal comfort over an urban airshed in India under varying land use/land cover conditions, Geoscience Letters 5 (27) (2018) 19pp.
[12] O. Brousse, A. Martilli, M. Foley, G. Mills, B. Bechtel, WUDAPT, an efficient land use producing data tool for mesoscale models? Integration of urban LCZ in WRF over Madrid, Urban Climate 17 (2016) 116–134.
[13] M. Bruse, H. Fleer, Simulating surface-plant-air interactions inside urban environments with a three dimensional numerical model, Environ. Model. Software 13 (3–4) (1998) 373–384.
[14] California Environmental Protection Agency, Preparing California for extreme heat: guidance and recommendations. http://www.climatechange.ca.gov/climate_action_team/reports/Preparing_California_for_Extreme_Heat.pdf, 2013 accessed 17.04.15.
[15] California Department of Public Health, Climate change and public health profile report- Santa Clara county. http://www.cdph.ca.gov/Programs/OHE/CDPH%20Document%20Library/CHORs/CHPR085SantaClara_County2-23-17.pdf, 2016 accessed 17.04.15.
[16] Y. Chen, N.H. Wong, Thermal benefits of city parks, Energy Build. 38 (2006) 105–120.
[17] F. Chen, H. Kusaka, R. Bornstein, J. Ching, C.S.B. Grimmond, S. Grossman-Clarke, T. Loridan, K. Manning, A. Martilli, S. Miao, D. Sailor, F. Salamaca, H. Taha, M. Tewari, X. Wang, A. Wyszogrodzki, C. Zhang, The integrated WRF/urban modelling system: development, evaluation, and applications to urban environmental problems, Int. J. Climatol. 31 (2) (2011) 273–288.
[18] W.T.L. Chow, R.L. Pope, C.A. Martin, A.J. Brazel, Observing and modeling the nocturnal park cool island of an arid city: horizontal and vertical impacts, Theor. Appl. Climatol. 103 (2011) 197–211.
[19] W.T.L. Chow, A.J. Brazel, Assessing xeriscaping as a sustainable heat island mitigation approach for a desert city, Build. Environ. 47 (2012) 170–181.
[20] P. Conry, A. Sharma, M. Potosnak, L. Leo, E. Bensman, J. Hellman, H. Fernando, Chicago's heat island and climate change: bridging the scale via dynamical downscaling, Journal of Applied Meteorology and Climatology 54 (7) (2015) 1430–1448.
[21] D. Crawley, L. Lawrieb, F. Winkelmannc, W.F. Buhlc, J. Huangc, et al., EnergyPlus: creating a new-generation building energy simulation program, Energy Build. 33 (2011) 319–331.
[23] M.B. Ek, K.E. Mitchell, Y. Lin, E. Rogers, P. Grunmann, V. Koren, J.D. Tarpley, Implementation of NOAH land surface model advances in the National Centers for Environmental Prediction operational mesoscale Eta model, J. Geophys. Res. 108 (D22) (2003), 8851.
[24] R. Emmanuel, H.J.S. Fernando, Urban heat islands in humid and arid climates: role of urban form and thermal properties in Colombo, Sri Lanka and Phoenix, USA, Clim. Res. 34 (2007) 241–251.
[25] H. Fernando, S.M. Lee, J. Anderson, M. Princevac, E. Pardyjak, S. Grossman-Clarke, Urban Fluid Mechanics: air circulation and contaminant dispersion in cities, Environ. Fluid Mech. 1 (2001) 107–164.
[26] T. Frank, Climate change impacts on building heating and cooling energy demand in Switzerland, Energy Build. 37 (11) (2005) 1175–1185.
[27] J. Geletič, M. Lehnert, P. Dobrovolný, Land surface temperature differences within local climate zones, based on two central European cities, Rem. Sens. 8 (10) (2016), 788.
[28] S. Hajat, T. Kosatky, Heat-related mortality: a review and exploration of heterogeneity, J. Epidemiol. Community 64 (9) (2010) 753–760.
[29] S. Huttner, Further Development and Application of the 3D Microclimate Simulation ENVI-Met. PhD Dissertation, University of Mainz, 2012.
[30] B. Jänicke, F. Meier, M.T. Hoelscher, D. Scherer, Evaluating the effects of façade greening on human bioclimate in a complex urban environment, Advances in Meteorology 2015 (2015) 15pp.
[31] Z.I. Janjic, The step-mountain Eta coordinate model: further developments of the convection, viscous layer, and turbulence closure schemes, Mon. Weather Rev. 122 (5) (1994) 927–945.
[32] R. Judkoff, B. Polly, M. Bianchi, J. Neymark, M. Kennedy, Building Energy Simulation Test for Existing Homes (BESTEST-EX): Instructions for Implementing the Test Procedure, Calibration Test Reference Results, and Example Acceptance-Range Criteria, NREL Report, 2011. No TP-5500-52414.
[33] C. Ketterer, A. Matzarakis, Human-biometeorological assessment of heat stress reduction by replanning measures in Stuttgart, Germany, Landsc. Urban Plann. 12 (2014) 78–88.

[34] L. Kleerekoper, M. Taleghani, A. van den Dobbelsteen, T. Hordijk, Urban measures for hot summer weather conditions in a temperate climate condition: a review study, Renew. Sustain. Energy Rev. 75 (2017) 515–533.
[35] H. Kusaka, H. Kondo, Y. Kikegawa, F. Kimura, A simple single-layer urban canopy model for atmospheric models: comparison with multi-layer and slab models, Boundary-Layer Meteorol. 101 (3) (2001) 329–358.
[36] H. Lee, H. Mayer, Validation of the mean radiant temperature simulated by the RayMan software in urban environments, Int. J. Biometeorol. 60 (11) (2016) 1775–1785.
[37] H. Lee, H. Mayer, L. Chen, Contribution of trees and grasslands to the mitigation of human heat stress in a residential district of Freiburg, Southwest Germany, Landsc. Urban Plann. 148 (2016) 37–50.
[38] Tj Lee, J.W. Yoo, H. Lee, H.S. Won, S.H. Lee, Study on the impacts of lateral boundary conditions and thermodynamics of urban park using coupling system of WRF/ENVI-met, Journal of Environmental Science International 26 (4) (2017) 493–507.
[39] F. Lindberg, B. Holmer, S. Thorsson, Solweig 1.0 – modelling spatial variations of 3D radiant fluxes and mean radiant temperature in complex urban settings, Int. J. Biometeorol. 52 (2008) 697–713.
[40] D. Liu, S. Hu, J. Liu, Contrasting the performance capabilities of urban radiation field between three microclimate simulation tools, Build. Environ. (2020), 175.
[41] G. Maggiotto, R. Buccolieri, M.A. Santo, L.S. Leo, S. Di Sabatino, Validation of temperature-pertur-bation and CFD-based modelling for the prediction of the thermal environment: the Lecce (IT) case study, Environ. Model. Software 60 (2014) 69–83.
[42] A. Martilli, A. Clappier, M.W. Rotach, An urban surface exchange parameterization for mesoscale models, Boundary-Layer Meteorol. 104 (2) (2002) 261–304.
[43] N. Müller, W. Kuttler, A.B. Barlag, Counteracting urban climate change: adaptation measures and their effect on thermal comfort, Theor. Appl. Climatol. 115 (2014) 243–257.
[44] E. Naboni, M. Meloni, S. Coccolo, J. Kaempf, J.L. Scartezzini, An overview of simulation tools for predicting the mean radiant temperature in an outdoor space, Energy Procedia 122 (2017) 1111–1116.
[45] N. Nazarian, J. Kleissl, CFD simulation of an idealized urban environment: thermal effects of geometrical characteristics and surface materials, Urban Climate 12 (2015) 141–159.
[46] E. Ng, L. Chen, Y. Wang, C. Yuan, A study on the cooling effects of greening in a high-density city: an experience from Hong Kong, Build. Environ. 47 (2012) 256–271.
[47] C. Ren, R. Wang, M. Cai, Y. Xu, Y. Zheng, E. Ng, The Accuracy of LCZ Maps Generated by the World Urban Database and Access Portal Tools (WUDAPT) Method: A Case Study of Hong Kong, 4th International Conference Countermeasure Urban Heat Islands, 2016. Singapore.
[48] L. Rui, R. Buccolieri, Z. Gao, E. Gatto, W. Ding, Study of the effect of green quantity and structure on thermal comfort and air quality in an urban-like residential district by ENVI-met modelling, Building Simulation 12 (2019) 183–194.
[49] M.A. Ruiz, E.N. Correa, Suitability of different comfort indices for the prediction of thermal conditions in tree-covered outdoor spaces in arid cities, Theor. Appl. Climatol. 122 (1–2) (2014) 69–83.
[50] F. Salamanca, A. Krpo, A. Martilli, A. Clappier, A new building energy model coupled with an urban canopy parameterization for urban climate situations – Part I. formulation, verification and sensitivity analysis of the model, Theor. Appl. Climatol. 9 (3–4) (2010) 331–344.
[51] T. Sharmin, K. Steemers, A. Matzarakis, Microclimatic modelling in assessing the impact of urban geometry on urban thermal environment, Sustainable Cities and Society 34 (2017) 293–308.
[52] L. Shashua-Bar, I.X. Tsiros, M. Hoffman, Passive cooling design options to ameliorate thermal comfort in urban streets of a Mediterranean climate (Athens) under hot summer conditions, Build. Environ. 57 (2012) 110–119.
[53] T. Shen, D.H.C. Chow, J. Darkwa, Simulating the influence of microclimatic design on mitigating Urban Heat Island effect in the Hangzhou Metropolitan area of China, Int. J. Low Carbon Technol. 11 (1) (2014) 130–139.
[54] H. Simon, J. Linden, D. Hoffmann, P. Braun, M. Bruse, J. Esper, Modeling transpiration and leaf temperature of urban trees – a case study evaluating the microclimate model ENVI-met against measurement data, Landsc. Urban Plann. 174 (2018) 33–40.
[55] W.C. Skamarock, J.B. Klemp, J. Dudhia, D.O. Gill, D.M. Barker, M.G. Duda, X. Huang, W. Wang, J.G. Powers, A Description of the Advanced Research WRF Version 3. NCAR. – Technical Report, Mesoscale and Microscale Meteorology Division, National Center for Atmospheric Research, Boulder, Colorado, USA, 2008.
[56] B. Song, S. Jung, Validation of ENVI-met model with in situ measurements considering spatial characteristics of land use types, Journal of the Korean association of geographic information studies 17 (2) (2014) 156–172.
[57] I.D. Stewart, A systematic review and scientific critique of methodology in modern urban heat island literature, Int. J. Climatol. 31 (2) (2011) 200–217.
[58] I.D. Stewart, T.R. Oke, Local climate zones for urban temperature studies, Bull. Am. Meteorol. Soc. 93 (12) (2012) 1879–1900.
[59] M. Taleghani, M. Tenpierik, A. Van Den Dobbelsteen, D.J. Sailor, Heat in courtyards: a validated and calibrated parametric study of heat mitigation strategies for urban courtyards in The Netherlands, Sol. Energy 103 (2014) 108–124.
[60] S. Tsoka, K. Tsikaloudaki, T. Theodosiou, D. Bikas, Urban warming and cities' microclimates: investigation methods and mitigation strategies – a review, Energies 13 (6) (2020) 25pp.
[61] UN-Habitat, State of the World's Cities 2012/2013, Prosperity of Cities. http://unhabitat.org/books/prosperity-of-cities-state-of-the-worlds-cities-20122013, 2013 accessed 18.04.01.
[62] P.E.J. Vos, B. Maiheu, J. Vankerkom, S. Janssen, Improving local air quality in cities: to tree or not to tree? Environ. Pollut. 183 (2013) 113–122.
[63] Y. Wang, U. Berardi, H. Akbari, Landscape modification for ambient environmental improvement in central business districts – a case from Beijing, Urban For. Urban Green. 14 (2015) 8–18.
[64] Y. Wang, D. Zhou, Y. Wang, Comparative study of urban residential design and microclimate characteristics based on ENVI-met simulation, Indoor Built Environ. 28 (9) (2019) 1200–1216.
[65] Q.H. Weng, D. Lu, J. Schubring, Estimation of land surface temperature-vegetation abundance relationship for urban heat island studies, Remote Sens. Environ. 89 (2004) 467–483.
[66] Z. Wu, P. Dou, L. Chen, Comparative and combinative cooling effects of different spatial arrangements of buildings and trees on microclimate, Sustainable Cities and Society 51 (2019) 9pp.
[68] X Yang, L Zhao, M Bruse, Q Meng, Evaluation of a microclimate model for predicting the thermal behavior of different ground surfaces, Building and Environment 60 (2013) 93–104.

GLOSSARY: Symbols and Acronyms

Greek Symbols

A: Albedo
Δt: Time step of integration
ΔT: Air temperature difference
ϵ: Surface emissivity
μ: Mean
P: Density
T: Solar transmissivity
Σ: Standard deviation

Roman Symbols

A: Absorptivity
c_p: Specific heat
C: Heat capacity
dd: Wind direction
Q: Specific humidity
H: Building height
H: Height of PBL top
K: Soil thermal conductivity
R: Solar radiation
RH: Relative humidity
T: Temperature
V: Wind speed
z_0: Roughness length

Acronyms

BC: Boundary Condition
BEM: Building Energy Model
BEP: Building Energy Parameterization
CAM: Community Atmosphere Model
CFD: Computational Fluid Dynamics
IC: Initial Condition
LCZ: Local Climate Zone
LST: Local Standard Time
LT1: Landsat-8 Level-1
LU/LC: Land-use/Land-cover
MMM: Mesoscale Meteorological Model
NAM: North American Mesoscale
NIR: Near Infrared Bands
NWS: National Weather Service
OIA: Oakland International Airport
PBL: Planetary Boundary Layer
PVC: Polyvinyl Chloride
ROI: Region of Interest
SCV: Santa Clara Valley
SJ: San Jose
SJA: San Jose International Airport
SJSU: San Jose State University
SLUCM: Single Layer Urban Canopy Model
SWIR: Shortwave Infrared Bands
TIR: Thermal Band
TKE: Turbulent Kinetic Energy
UHI: Urban Heat Island
USGS: United States Geological Survey
uWRF: Urbanized WRF
WRF: Weather Research and Forecasting Model
WUDAPT: World Urban Database and Access Portal Tools